Pergamon

0301-9322(94)E0011-7

Int. J. Multiphase Flow Vol. 20, Suppl., pp. 387–414, 1994

0301-9322/94 $26.00 + 0.00

INTERFACIAL AND STRUCTURAL STABILITY OF SEPARATED FLOW

D. BARNEA and Y. TAITEL

Department of Fluid Mechanics and Heat Transfer, Faculty of Engineering, Tel-Aviv University, Ramat-Aviv 69978, Israel

(Received 9 February 1994)

Abstract—An overview on the stability of separated flow (stratified and annular flow) is presented. The stability of separated flows is discussed using two approaches: the interfacial stability analysis and the structural stability analysis. For each case the stability of the steady state solutions has been examined, using linear and non-linear analyses.

Both the interfacial and the structural stability analyses are needed for the complete information regarding the stability of the steady state solutions and the resulting flow pattern transition.

Key Words: two-phase flow, stability, flow pattern, stratified flow, annular flow

INTRODUCTION

Gas–liquid flow in pipes can adopt different flow configurations, depending on the distribution of the gas–liquid interface. The four basic flow patterns are stratified, intermittent, annular and bubble flows. Separated flow is defined as the flow pattern where there is continuity of both phases in the axial direction. This condition is satisfied for stratified flow for which the liquid flows at the bottom of the pipe and the gas flows above it, and for annular flow where the liquid film flows along the pipe periphery and the gas flows in the core. The interest in separated flow is not limited to the study of the stratified or annular flow parameters, it is also used as a vehicle for analyzing the transition from separated flow to other flow patterns by examining the stability of the separated flow and the possible instability that may lead to transition.

The stability of stratified flow is a very complex phenomenon and it is studied, on the one hand, in connection with the generation of waves on the interface and, on the other hand, in connection with the transition from stratified flow into intermittent or annular flow. The approach to such instability analysis can be classified into several categories: linear vs non-linear, inviscid vs viscous and one-dimensional analysis vs two (or multi)-dimensional analysis. Comprehensive reviews on this subject have been given by Hanratty (1983) and Hanratty & McCready (1992).

Waves generated on an interface owing to interfacial instability can either lead to a wavy interface or to conditions where the waves reach the top of the pipe and cause transition from stratified flow. Interest in the stability of stratified flow covers both these aspects. Usually, it is conceded that instability which leads to the growth of short waves will result in pebbly flow, since short waves saturate quickly and their effect is to roughen the surface and increase the interfacial shear stress rather than cause transition (Bruno & McCready 1988; Hanratty & McCready 1992). On the other hand, long-wave instability is associated with the generation of roll waves which, under certain conditions, may grow and result in the transition form stratified flow to intermittent or annular flow.

Jeffreys (1925) attributed the generation of waves to the "wind action" on the wave slope. Andritsos & Hanratty (1987) also mentioned that pebbled waves are indeed caused by the wind action, i.e. the imbalance between the wind energy fed to the waves and the viscous dissipation. Roll waves, on the other hand, occur when the destabilizing effect of the liquid inertia and pressure variation over long waves, which are in phase with the wave height, overcomes gravity (Hanratty & Hershman 1961; Andreussi *et al.* 1985). Atomization is suggested to take place as a result of the pressure variation overcoming the surface tension.

We are interested in focusing attention on those mechanisms that lead to the transitions from stratified flow to intermittent or annular flow and from annular flow to slug or dispersed bubble flow. The instability which causes transition from stratified flow is usually attributed to the Kelvin–Helmholtz (KH) instability.

The KH instability results primarily from the Bernoulli effect, i.e. the decrease in the pressure over the wave crest due to the velocity acceleration. This destabilizing effect acts against the stabilizing effect of gravity. Exact three-dimensional analysis of the KH instability is difficult if the viscosity and circular geometry are considered. However, the waves we are interested in are long waves, since only they generate large-amplitude waves (roll waves) and cause transition. Thus, the long wave, one-dimensional, theory is well-suited to analyzing the instability that may lead to transition from stratified flow. In this case the starting point is the two-fluid model equations, also termed the "one-dimensional" formulation, rather than the full Navier–Stokes equations.

The linear stability analysis of the "one-dimensional" equations is presented in Wallis's (1969) book. It is concluded that the point of instability occurs when the kinematic wave and the dynamic wave have the same speed. Crowley *et al.* (1992) used this criterion to predict transition from stratified flow. Lin & Hanratty (1986, 1987) distinguished between the viscous Kelvin–Helmholtz (VKH) and the inviscid Kelvin–Helmholtz (IKH) analysis and observed that the VKH analysis predicts well the transition to roll waves on thin liquid layers and the transition to slug flow for high liquid layers (low gas velocity). Wu *et al.* (1987) used the VKH analysis to predict transition from stratified flow for high-pressure and large-diameter pipes. Barnea (1991a) and Barnea & Taitel (1993) noticed that neither the VKH nor the IKH theories by themselves provide an adequate solution for the prediction of the transition boundary from stratified flow to intermittent and annular flows for all pipe inclinations. A combined model that incorporates both the VKH and the IKH analyses and the equilibrium void fraction was proposed for the prediction of the transition boundary from stratified flow to slug flow, to annular flow and also to roll waves (Barnea 1991a).

Wallis & Dobson (1973) and Taitel & Dukler (1976) proposed a simplified IKH analysis, which incorporates an empirical constant to fit the theory to the experimental results. These approaches provide a simple means for the prediction of the transition boundary and usually their results compare reasonably well with experiments and with the more accurate VKH and IKH analyses. Owing to the simplicity of the method it is widely used. Andreussi & Persen (1987) used the Taitel & Dukler (1976) model successfully but took into account more accurate effective shear stresses obtained by an empirical relation. Kordyban & Ranov (1970) proposed a stratified/slug transition boundary that is based on the inverse Benjamin (1968) model. Mishima & Ishii (1980) used an inviscid two-dimensional analysis of a flat geometry and developed a criterion for the onset of slug flow in a horizontal duct using the concept of the "most dangerous wave".

In the case of annular flow, the interface is always unstable to KH analysis hence the transition from annular flow should be treated differently. Barnea & Taitel (1989, 1990) proposed a different kind of instability, termed "structural instability". Structural stability analysis indicates whether the typical structure of separated flow is maintained; namely, whether the steady-state solutions are stable structures with respect to the average film thickness, even when the interface is unstable to KH and is wavy. Structural stability analysis can be applied to annular flow as well as to stratified flow. It is used to distinguish between steady-state solutions that will actually take place and unstable solutions that will not exist. For the flow pattern transition, both the structural and KH analyses should be considered (Barnea & Taitel 1992).

This review article covers the topic of long-wave instability. It is detailed enough to be self-consistent and to minimize the need to refer to the original papers. Different authors use their own style and format, even when referring to the same basic theory. In this article, naturally, we adhere to our own style, which we feel also constitutes a simpler presentation compared with the work of most authors.

In the first part of this article, long-wave interfacial instability is examined. The linear VKH and IKH instability analyses are presented and their interpretation for the flow pattern transition is discussed. Further, non-linear simulations are performed to examine the behavior of waves beyond the linear range. In the second part, the structural analysis is presented and its application to the stability of annular flow and stratified flow is discussed. Both linear and non-linear analyses are considered.

INTERFACIAL STABILITY

The first step in analyzing the stability of separated two-phase flow and developing transition criteria is to predict the equilibrium liquid level. The commonly used method for calculating the steady-state liquid level in stratified flow, or the film thickness in annular flow, is to use the one-dimensional approach, which treats the gas and the liquid as two separated fluids with average and constant cross-sectional areas along the pipe and with constant average gas and liquid velocities, U_G and U_L. Since information regarding the local gradients and interfacial distribution is lost, effective wall and interfacial shear stresses are required in order to replace this information. The solution of the liquid level in this case is for the average level. The transient formulation which is consistent with the aforementioned steady-state solutions is provided by the "two-fluid model". In the following, the "two-fluid model" will be used to analyze the linear and non-linear stability of the interface.

Interfacial Linear Stability

The stability of the steady-state solutions is usually checked by the classical linear KH stability analysis. For long-wave analysis (one-dimensional approach) two types of KH analyses have been used: the viscous Kelvin–Helmholtz (VKH) analysis, which uses the full two-fluid model and takes into account the shear stresses (Wallis 1969; Lin & Hanratty 1986; Wu *et al.* 1987; Andritsos *et al.* 1989; Barnea 1991a; Crowley *et al.* 1992); and the inviscid Kelvin–Helmholtz (IKH) theory, in which the shear stresses are neglected (Taitel & Dukler 1976; Kordyban 1977; Wallis & Dobson 1973; Mishima & Ishii 1980). Note, that in both analyses the steady equilibrium liquid level, about which the stability is examined, is obtained taking the shear stresses into account.

The key question is how to interpret the behavior in the unstable region due to both the viscous and inviscid analyses. Do these instabilities result in the transition to slug flow or annular flow, or just cause the interface to be wavy? The following sections attempt to address these questions.

The viscous (VKH) and inviscid Kelvin–Helmholtz (IKH) analyses

The VKH stability analysis is performed on the two-fluid model equations.

The continuity equations for the liquid and for the gas are:

$$\frac{\partial}{\partial t}(\rho_L A_L) + \frac{\partial}{\partial x}(\rho_L A_L U_L) = 0 \qquad [1]$$

and

$$\frac{\partial}{\partial t}(\rho_G A_G) + \frac{\partial}{\partial x}(\rho_G A_G U_G) = 0. \qquad [2]$$

The momentum equations for each phase are:

$$\frac{\partial}{\partial t}(\rho_L A_L U_L) + \frac{\partial}{\partial x}(\rho_L A_L U_L^2) = -\tau_L S_L + \tau_i S_i - A_L \frac{\partial P_{iL}}{\partial x} - \rho_L A_L g \cos\beta \frac{\partial h_L}{\partial x} - \rho_L A_L g \sin\beta \qquad [3]$$

and

$$\frac{\partial}{\partial t}(\rho_G A_G U_G) + \frac{\partial}{\partial x}(\rho_G A_G U_G^2) = -\tau_G S_G - \tau_i S_i - A_G \frac{\partial P_{iG}}{\partial x} - \rho_G A_G g \cos\beta \frac{\partial h_L}{\partial x} - \rho_G A_G g \sin\beta, \qquad [4]$$

where A is the cross-sectional area, h is the liquid level or gas gap, P is the pressure, U is the axial average velocity, τ is the shear stress, S is the perimeter over which τ acts, ρ is the phase density and β is the angle of inclination from the horizontal (positive for upward flow); the subscripts L and G denote liquid and gas, respectively, and the subscript i denotes the interface.

Assuming incompressible flow and combining the two momentum equations by eliminating the pressure terms using the approximate relation

$$P_{Gi} - P_{Li} = \sigma \frac{\partial^2 h_L}{\partial x^2}, \qquad [5]$$

where σ is the surface tension, yields the following three equations:

$$\frac{\partial h_L}{\partial t} + \frac{A_L}{A'_L}\frac{\partial U_L}{\partial x} + U_L\frac{\partial h_L}{\partial x} = 0 \qquad [6]$$

$$\frac{\partial h_L}{\partial t} - \frac{A_G}{A'_L}\frac{\partial U_G}{\partial x} + U_G\frac{\partial h_L}{\partial x} = 0 \qquad [7]$$

and

$$\rho_L\frac{\partial U_L}{\partial t} - \rho_G\frac{\partial U_G}{\partial t} + \rho_L U_L\frac{\partial U_L}{\partial x} - \rho_G U_G\frac{\partial U_G}{\partial x} + (\rho_L - \rho_G)g\cos\beta\frac{\partial h_L}{\partial x} - \sigma\frac{\partial^3 h_L}{\partial x^3} = F, \qquad [8]$$

where

$$F = -\frac{\tau_L S_L}{A_L} + \frac{\tau_G S_G}{A_G} + \tau_i S_i\left(\frac{1}{A_L} + \frac{1}{A_G}\right) - (\rho_L - \rho_G)g\sin\beta \qquad [9]$$

and A'_L is dA_L/dh_L.

Setting $F = 0$ yields the steady-state solutions. Linearizing [6]–[8] about the steady-state solution and substituting for the perturbed liquid level,

$$\hat{h}_L = \epsilon\exp[i(\omega t - kx)], \qquad [10]$$

into the linearized equations, yields the following dispersion equation for the angular frequency, ω:

$$\omega^2 - 2(ak - bi)\omega + ck^2 - dk^4 - eki = 0, \qquad [11]$$

where

$$a = \frac{1}{\rho}\left(\frac{\rho_L U_L}{R_L} + \frac{\rho_G U_G}{R_G}\right), \qquad [12a]$$

$$b = \frac{1}{2\rho}\left[\left(\frac{\partial F}{\partial U_{LS}}\right)_{U_{GS},R_L} - \left(\frac{\partial F}{\partial U_{GS}}\right)_{U_{LS},R_L}\right], \qquad [12b]$$

$$c = \frac{1}{\rho}\left[\frac{\rho_L U_L^2}{R_L} + \frac{\rho_G U_G^2}{R_G} - (\rho_L - \rho_G)g\cos\beta\frac{A}{A'_L}\right], \qquad [12c]$$

$$d = \frac{\sigma}{\rho}\frac{A}{A'_L}, \qquad [12d]$$

$$e = -\frac{1}{\rho}\left(\frac{\partial F}{\partial R_L}\right)_{U_{LS},U_{GS}}, \qquad [12e]$$

$$\rho = \frac{\rho_L}{R_L} + \frac{\rho_G}{R_G} \qquad [12f]$$

U_{LS}, U_{GS} are the liquid and gas superficial velocities, $R_L = A_L/A$ and $R_G = A_G A$.

All the variables in [12a–f] are in the steady-state conditions. The solution for ω is

$$\omega = (ak - bi) \pm \sqrt{(a^2 - c)k^2 - b^2 + dk^2 + (ek - 2abk)i}. \qquad [13]$$

The steady-state solution is unstable whenever the imaginary part of ω in [13], namely ω_I, is negative, leading to exponential growth of the perturbed variable, $\hat{h}_L$. The amplification factor is $-\omega_I$.

For the inviscid case a simple expression for ω is obtained:

$$C = \frac{\omega}{k} = \frac{\dfrac{\rho_L U_L}{H_L} + \dfrac{\rho_G U_G}{H_G}}{\dfrac{\rho_L}{H_L} + \dfrac{\rho_G}{H_G}} \pm \sqrt{\frac{(\rho_L - \rho_G)g\cos\beta}{\dfrac{\rho_L}{H_L} + \dfrac{\rho_G}{H_G}} - \frac{\dfrac{\rho_L\rho_G}{H_L H_G}(U_G - U_L)^2}{\left(\dfrac{\rho_L}{H_L} + \dfrac{\rho_G}{H_G}\right)^2} + \frac{\sigma k^2}{\dfrac{\rho_L}{H_L} + \dfrac{\rho_G}{H_G}}}, \qquad [14]$$

where $H_L = A_L/A'_L$ and $H_G = A_G/A'_G$ ($A'_G = dA_G/dh_G$); C is the wave velocity and k is the wavenumber. As long as the term in the square root is positive, the amplification factor in this case is zero. When the square root is negative, two conjugate solutions for the imaginary part exist. The second solution—namely, the one with the negative sign—is the one that contributes to the instability.

For the viscous case, the solution for ω can be expressed conveniently in polar form:

$$\omega_1 = (ak - bi) + \sqrt[4]{\alpha^2 + \gamma^2}\exp\left[i\tfrac{1}{2}\arctan\left(\frac{\gamma}{\alpha}\right)\right] \quad [15]$$

and

$$\omega_2 = (ak - bi) + \sqrt[4]{\alpha^2 + \gamma^2}\exp\left\{i\frac{1}{2}\left[\arctan\left(\frac{\gamma}{\alpha}\right) + 2\pi\right]\right\}, \quad [16]$$

where $\alpha = (a^2 - c)k^2 + dk^4 - b^2$ and $\gamma = ek - 2abk$. The negative value of the imaginary part of [16] is the amplification factor.

The condition for marginal stability can be found from [11] for the special case where ω_1, the imaginary part, equals zero. This leads to the following stability criterion for the viscous case:

$$\left(\frac{e}{2b} - a\right)^2 - (a^2 - c) - dk^2 < 0; \quad [17]$$

substituting the value of $a^2 - c$ from [12a, c] into [17] yields

$$(C_V - C_{IV})^2 + \frac{\rho_L \rho_G}{\rho^2 R_L R_G}(U_G - U_L)^2 - \frac{\rho_L - \rho_G}{\rho} g \cos\beta \frac{A}{A'_L} - \frac{\sigma}{\rho}\frac{A}{A'_L}k^2 < 0 \quad [18]$$

The last three terms on the LHS of [18] comprise the stability criterion for the inviscid analysis, where the viscous effects are neglected. The first term is the additional effect of the shear stresses, which tend to amplify any disturbance in the film thickness. Note that the fourth term, which is the contribution of the surface tension, is the only term that depends on the wavelength. For long waves this term approaches zero and does not affect the neutral stability criterion, which should apply to all wavelengths. Obviously, the same result is obtained if the surface tension is taken as zero.

C_V in [18] is the critical wave velocity on the inception of instability,

$$C_V = \frac{e}{2b} = \frac{\left(\dfrac{\partial F}{\partial R_L}\right)_{U_{LS}, U_{GS}}}{\left[\left(\dfrac{\partial F}{\partial U_{GS}}\right)_{U_{LS}, R_L} - \left(\dfrac{\partial F}{\partial U_{LS}}\right)_{U_{GS}, R_L}\right]}; \quad [19]$$

and C_{IV} is the critical wave velocity for the IKH analysis,

$$C_{IV} = \frac{\rho_L U_L R_G + \rho_G U_G R_L}{\rho_L R_G + \rho_G R_L}. \quad [20]$$

In this work, the shear stresses τ_L, τ_G and τ_i are evaluated as follows:

$$\tau_L = f_L \frac{\rho_L U_L^2}{2}, \quad [21]$$

$$\tau_G = f_G \frac{\rho_G U_G^2}{2} \quad [22]$$

and

$$\tau_i = f_i \frac{\rho_G (U_G - U_L)|U_G - U_L|}{2}, \quad [23]$$

where

$$f_L = C_L\left(\frac{D_L U_L}{\upsilon_L}\right)^{-n} \quad \text{and} \quad f_G = C_G\left(\frac{D_G U_G}{\upsilon_G}\right)^{-m}. \quad [24]$$

D_L and D_G are the hydraulic diameters, evaluated in the following manner:

$$D_L = \frac{4A_L}{S_L} \quad \text{and} \quad D_G = \frac{4A_G}{S_G + S_i}. \tag{25}$$

The coefficients C_G and C_L equal 0.046 for turbulent flow and 16 for laminar flow, n and m take the values of 0.2 for turbulent flow and 1.0 for laminar flow. The interfacial friction factor is assumed to have a constant value of $f_i = 0.014$, as suggested by Cohen & Hanratty (1968), for stratified wavy flow, or $f_i = f_G$ when $f_G > 0.014$.

The KH criterion for neutral stability [18] (for long wavelength) can be rearranged in the following form:

$$(U_G - U_L) < K\left[(\rho_L R_G + \rho_G R_L)\frac{\rho_L - \rho_G}{\rho_L \rho_G} g \cos\beta \frac{A}{\frac{dA_L}{dh_L}}\right]^{1/2} \tag{26}$$

For the inviscid case, the factor $K = 1$; for the viscous case, $K = K_V$, where

$$K_V = \sqrt{1 - \frac{(C_V - C_{IV})^2}{\frac{\rho_L - \rho_G}{\rho} g \cos\beta \frac{A}{\frac{dA_L}{dh_L}}}}. \tag{27}$$

Taitel & Dukler (1976) used a simplified inviscid analysis. In order to account for finite waves, Taitel & Dukler suggested a speculative factor,

$$K = K_{TD} = 1 - \frac{h_L}{D}. \tag{28}$$

It turns out that this factor accounts successfully for the viscous effects also, especially at low viscosities.

Figure 1 compares the Taitel & Dukler factor $K_{TD} = 1 - h_L/D$ and the factor obtained in the present analysis, K_V [27], for the case of low-pressure air–liquid flow in horizontal pipes. The factors K_{TD} and K_V are calculated for the conditions of neutral stability. The dependence of the Taitel & Dukler factor on the superficial gas velocity at the inception of instability is not affected, in practice, by the liquid viscosity and the viscosity affects the inception of instability only via h_L/D. On the other hand, K_V is a strong function of the viscosity [27]. As the liquid viscosity increases, K_V approaches unity, and the solution obtained by the IKH analysis approaches the solution obtained by the VKH analysis. For the special case where the viscosity of the liquid is 1 cP, the curves of K_V and K_{TD} are almost identical, resulting in very similar transitional curves on the U_{LS}–U_{GS} map.

Figure 2 presents the results of the neutral stability criterion obtained by both the viscous and inviscid approaches, for three pipe inclinations (horizontal, upward inclined and downward inclined flows). The calculations were made for air and liquid at various viscosities in a 5 cm dia pipe. It can be seen that, for the low viscosities, the inviscid analysis overpredicts the viscous results considerably, especially for inclined pipes. For upward inclined flow and 1 cP liquid viscosity, for example, the stable area predicted by the VKH analysis is bounded by the bell-shaped curve, while

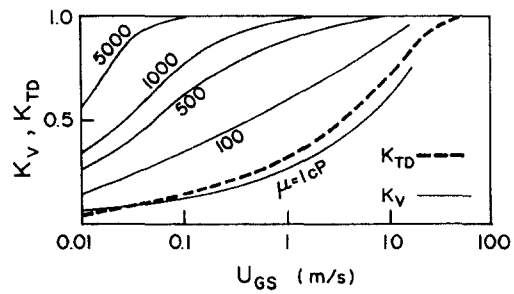

Figure 1. The influence of liquid viscosity on the coefficients K_V [27] and K_{TD} [28]. Air–liquid, atmospheric pressure, horizontal pipe, $D = 5$ cm.

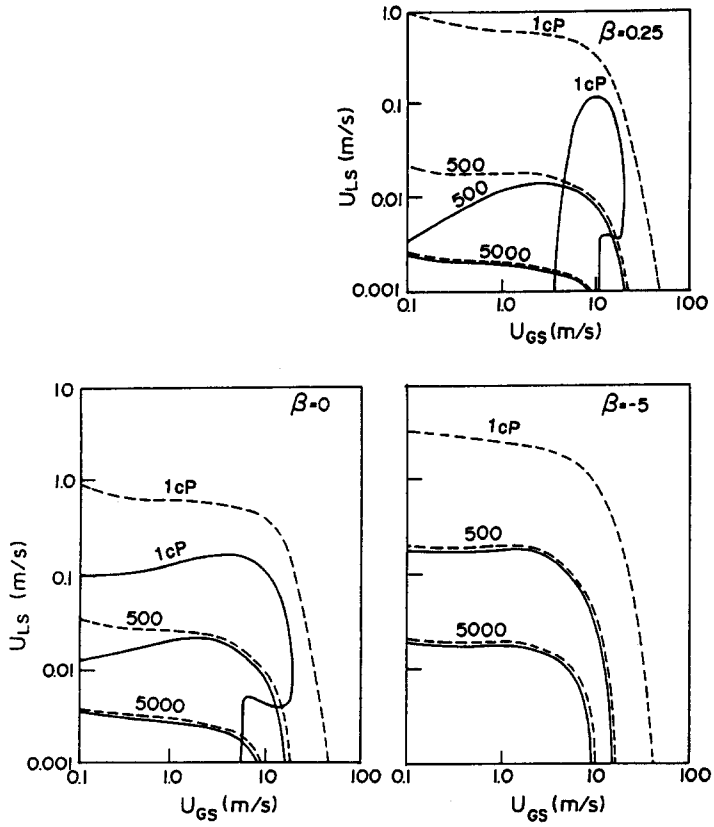

Figure 2. Effect of liquid viscosity on the neutral stability curves. Air–liquid, atmospheric pressure, $D = 5$ cm. ——, VKH; – – –, IKH.

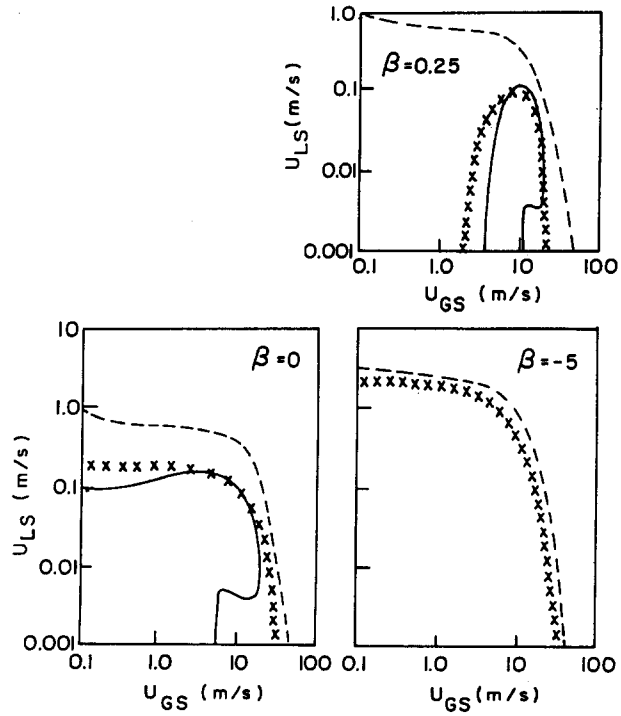

Figure 3. Comparison of the KH neutral stability curves with experimental data. Air–water, atmospheric pressure, $D = 5$ cm dia pipe. ——, VKH; – – –, IKH; × × ×, Exp. (Shoham 1982).

the stable zone due to the IKH analysis is much larger. For downward flow, the VKH analysis predicts unstable flow for the case of 1 cP for the whole range of flow rates presented here (the solid curve is missing), while the IKH analysis predicts a large stable zone. As the liquid viscosity increases, both approaches yield almost the same results.

The VKH and IKH neutral stability lines were checked for possible application as flow pattern transition boundaries. Figure 3 shows the results for the case of a low liquid viscosity of 1 cP. The region bounded by the solid lines is stable stratified flow due to the VKH analysis. The broken lines bound the stable region due to the IKH analysis and the region bounded by the $\times \times \times$ line is a region of stratified flow observed via experiments (Shoham 1982). It can be seen that the IKH instability does not predict well the transition boundaries from stratified flow for horizontal and upward flows, i.e. the stable region predicted by the IKH analysis is larger compared with the experimental data. The VKH neutral stability lines, on the other hand, compare quite well with the experimental transition boundaries from stratified flow for horizontal and upward inclined flow. However, at downward inclination the viscous analysis predicts unstable stratified flow, while the data indicate the existence of stratified flow in this range of flow rates. Thus, the neutral stability condition of the VKH analysis is not directly associated with the transition from stratified flow as well. It can be seen that neither the VKH nor the IKH by themselves are able to predict correctly the transition from stratified flow. The question to be addressed at this point is: what is the physical interpretation of the instabilities due to the VKH and the IKH analyses?

Hanratty (1983) and Andreussi *et al.* (1985) indicated that the VKH type of instability actually predicts the formation of an unstable interface with large-amplitude roll waves. Whenever the liquid level is high enough, the waves bridge the pipe and the unstable interface becomes slug flow. For thin films, on the other hand, either roll waves or annular flow may exist. To obtain annular flow, the upper part of the pipe should be wetted even if the film is thin. This occurs when the suction generated over the wave crest due to the Bernoulli effect overcomes the stabilizing influence of gravity. This effect is in phase with the wave height and the wave will grow unboundedly until the upper part of the pipe is wet. This description is consistent with the IKH analysis, where the instability is determined by the balance between the Bernoulli force and the gravity force. Thus, one assumes that the instability due to the IKH analysis results in an unbounded growth up to the top of the pipe. For high liquid films this unbounded growth will cause slug flow, while for thin films, where the liquid supply is too small to bridge the pipe, the result would be a wetted periphery, namely, annular flow.

Barnea (1991a) proposed a complete description of the behavior of the interface due to the viscous and the inviscid instabilities. Referring to figure 4, the region bounded by the VKH neutral stability line is a region of stable stratified flow (SS), namely, stratified smooth or stratified wavy flow with small-amplitude waves. Beyond this region, three regions of instability are identified. The region outside the VKH neutral stability line, for which the equilibrium liquid level is high, is a region of slug flow (SL). For the case of low liquid levels, the region which is unstable to the VKH and stable to the IKH analysis is a region of large-amplitude roll waves (RW) and the region of low liquid level which is unstable to the IKH analysis is in annular flow (A). In this work, the Taitel & Dukler (1976) suggestion of $h_L/D = 0.5$ is adopted to quantify a high liquid level.

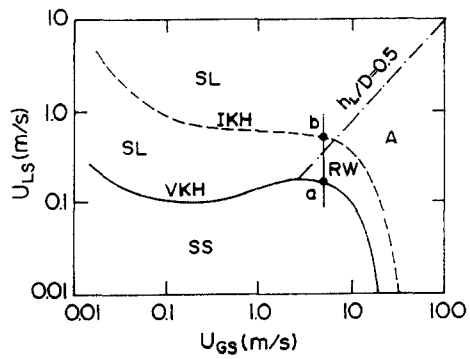

Figure 4. Flow pattern prediction by the VKH and the IKH analyses. Air–water, atmospheric pressure, horizontal pipe, $D = 5$ cm. SS—stable stratified, RW—roll waves, SL—slug, A—annular.

So far, the analysis of stratified flow has been based only on the neutral stability condition. It turns out that this is not sufficient to give a clear picture of the instability phenomenon. For example: one would expect the IKH theory to be a good approximation for low-viscosity liquids, whereas for high viscosities one would have to use the full two-fluid model, namely the VKH analysis, in order to get correct results. Surprisingly, the results are quite the opposite. For highly viscous liquids the results of the IKH theory are applicable, while there is a large discrepancy between the results of the IKH and VKH theories for low liquid viscosity. In addition, our physical interpretation of the VKH and IKH neutral stability lines is based only on physical intuition and we wish to enhance our general interpretation of the KH analyses for flow pattern transition with additional theoretical support. It is decided, therefore, to observe not only the condition when the disturbance becomes unstable but to consider also the rate of amplification of this disturbance (Barnea & Taitel 1993). The rate of amplification is examined along line a–b in figure 4. Point "a" is the intersection point with the VKH neutral stability curve, while point "b" is the intersection with the IKH neutral stability curve.

The dispersion equation [11] yields two solutions for ω_1. Positive or zero solutions indicate stable flow. For the viscous analysis, ω_{I1} is always positive, while ω_{I2} changes sign from positive (stable flow), for U_{LS} below point "a", to negative (unstable flow) above point "a". For the case of the IKH analysis, ω_{I1} and ω_{I2} are zero for U_{LS} below point "b". Above point "b", ω_{I2} is negative (unstable) and ω_{I1} is the positive conjugate of ω_{I2}. The value of $-\omega_{I2}$ is the rate of amplification of the disturbance and is illustrated in figure 5 as a function of the wavelength, for a constant gas flow rate ($U_{GS} = 5$ m/s) and various liquid flow rates (along line a–b in figure 4). The results obtained for the two analyses (the VKH and the IKH) are almost the same and they are indistinguishable in figure 5(I) (although the neutral stability criterion is quite different). An enlarged picture of the two solutions is shown in figure 5(II) to show the behavior at low amplification rates. In this figure, the details in the vicinity of neutral stability can be observed.

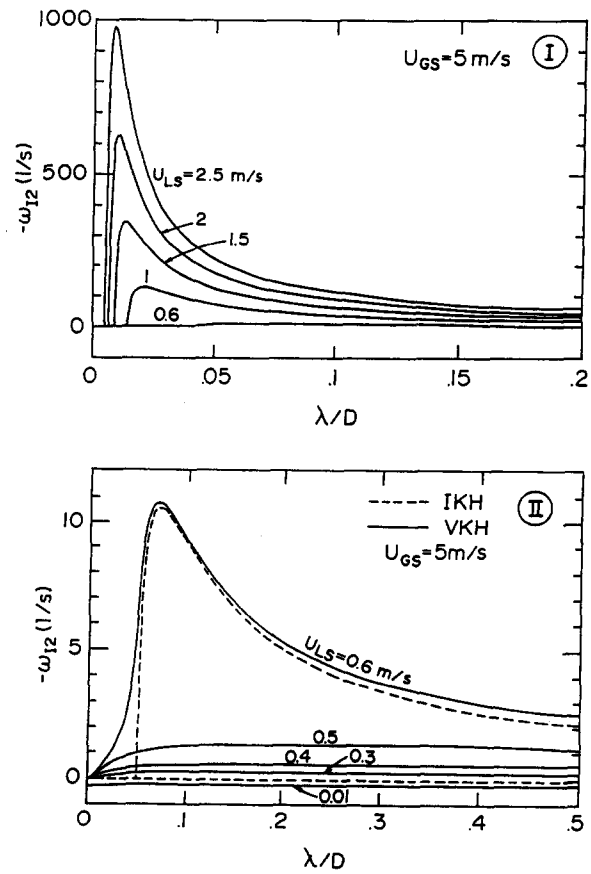

Figure 5. Amplification factor for air–water at $U_{GS} = 5$ m/s.

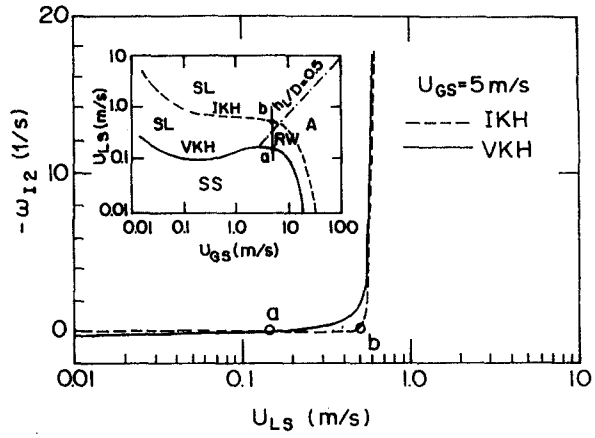

Figure 6. Maximal amplification factor for horizontal flow, $U_{GS} = 5$ m/s. Air–water, atmospheric pressure, $D = 5$ cm.

For liquid flow rates below point "a", $U_{LS} = 0.01$ m/s, $-\omega_{I2}$ is negative for all wavelengths according to the VKH analysis, namely the flow is stable. For U_{LS} between points "a" and "b", $-\omega_{I2}$ is positive with very low absolute values and only at $U_{LS} = 0.6$ m/s, where the flow becomes unstable according to the IKH analysis, does the rate of amplification become meaningful. Stated differently, under the flow conditions where the IKH analysis indicates a zero rate of amplification, the VKH analysis yields a transition from a negative to a positive value of $-\omega_{I2}$ with absolute values that are close to zero. The rate of amplification obtained by the VKH analysis is substantial only at conditions where the IKH analysis indicates unstable flow.

A convenient method for comparing the amplification factors for the two analyses with respect to the flow rates is to look at the amplification factor at a certain wavelength. This wavelength may be chosen arbitrarily. In this work we chose to compare the solutions at the wavelength which yields the maximum rate of amplification. Figure 6 shows the maximal rate of amplification at each liquid flow rate for a constant gas flow rate. It can be seen clearly, again, that from this point of view the stability behavior of the system is almost the same according to the two types of KH analysis. For the IKH case the amplification factor is exactly zero up to the neutral stability point, "b", where the amplification curve maintains a clearly visible positive slope. For the VKH case, the amplification factor is negative for very low liquid flow rates and becomes positive for increasing liquid flow rates with absolute values very close to zero. Point "a", where the amplification factor changes sign, is the neutral stability point for the VKH analysis. The sharp increase in the amplification factor for the VKH case occurs close to the same point as for the IKH case.

Figure 7 presents the effect of viscosity on the maximal amplification rate for both the VKH and IKH analyses. The amplification factors for both analyses are indistinguishable for the whole range

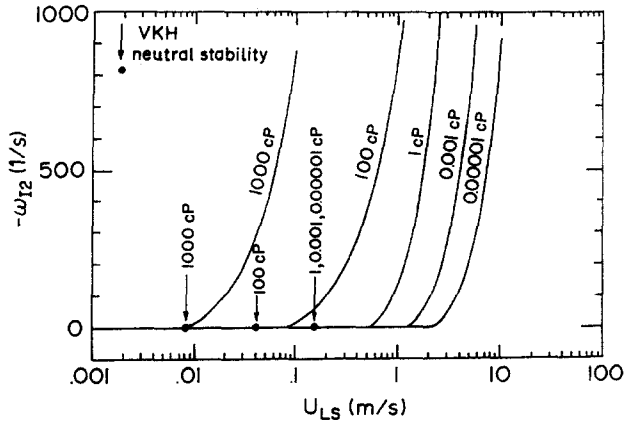

Figure 7. Effect of liquid viscosity on the amplification factor, $U_{GS} = 5$ m/s. Air–liquid, atmospheric pressure, horizontal pipe, $D = 5$ cm.

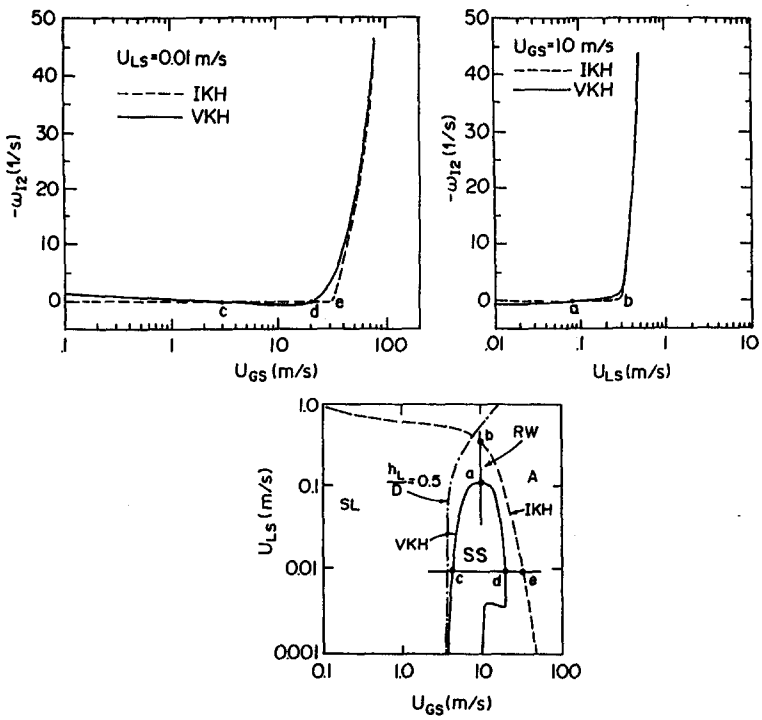

Figure 8. Maximal amplification factor for upward flow. Air–water, atmospheric pressure, $\beta = 0.25°$, $D = 5$ cm.

of liquid viscosities. Along the region where the IKH amplification rate is zero the VKH analysis yields very low amplification. The point of neutral stability due to VKH analysis, i.e. when the amplification factor changes signs, is designated in the figure by an arrow. It is interesting to observe that for high viscosities the neutral stability points for both analyses are at almost the same location, while for low viscosities the neutral stability points are quite far apart.

A similar behavior regarding the stability characteristics of the system is obtained for the case of inclined stratified flow. For upward inclined flow, the maximal amplification rate along a constant gas flow rate line (a–b) and along a constant liquid flow rate line (c–d–e) is illustrated in figure 8. Again, the amplification curves are very similar, although the neutral stability curves obtained by the two analyses are quite different. The results for the amplification factor along the line a–b are similar to the horizontal case. For the case of constant liquid flow rate (line c–d–e), the amplification factor is positive and small; for low gas flow rate, it becomes negative, signifying a stable interface, in the region from point "c" to "d", and thereafter a sharp increase in the

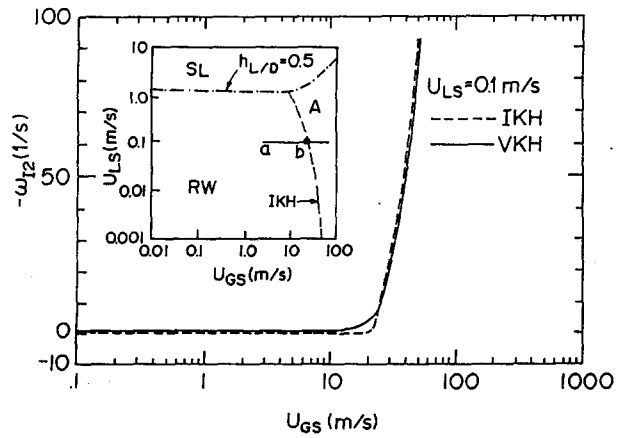

Figure 9. Maximal amplification factor for downwards inclined flow, $U_{LS} = 0.1$ m/s. Air–water, atmospheric pressure, $\beta = -5°$, $D = 5$ cm.

amplification factor is observed where the flow becomes unstable according to the IKH analysis (point e).

Figure 9 is a typical representation of the stability behavior for downward inclined stratified flow. The amplification factor curves for the two analyses again yield almost the same results. However, along the region where the IKH analysis predicts zero amplification (namely, neutral stability conditions) the flow is unstable according to the VKH analysis with a very small amplification rate. This means that, for this case, the VKH neutral stability line is absent and the transition from stratified flow is controlled only by the IKH neutral stability curve and $h_L/D = 0.5$. The whole region bounded by the aforementioned lines is, therefore, a region of stratified flow with roll waves.

The behavior of the amplification factor indeed supports our previous interpretation of the VKH and IKH neutral stability lines. The region bounded between the VKH and IKH neutral stability lines is a region of low amplification factor, which leads to the formation of large-amplitude roll waves. For high liquid levels, these roll waves will block the pipe, resulting in slug flow. On the other hand, the region outside the IKH neutral stability line is associated with very high amplification factors (by both analyses), inducing an unbounded growth of the disturbance which always results in the transition from stratified flow to annular flow for high void or to slug flow for low void.

The results for the amplification factors also explain well the dilemma of the neutral stability solutions for the VKH and IKH analyses being different for low liquid viscosity. As has been shown, the solutions for the amplification factors are very similar for the two analyses for low liquid viscosity. In the range where the IKH analysis predicts zero amplification, the VKH analysis predicts a very low amplification factor.

Non-linear Interfacial Stability

In the above, our physical interpretation regarding the flow pattern transition was based solely on the linear stability analyses (neutral stability lines and amplification factors for the VKH and IKH analyses). However, the linear analysis does not provide information as to the evolution of the interface up to the point of transition from stratified flow. Thus, the interpretation based on the linear results is somewhat speculative. Therefore, a non-linear stability analysis has been carried out using numerical simulation to examine the system response to finite disturbances of the interface.

Barnea & Taitel (1994) investigated the non-linear interfacial stability of stratified flow and confirmed most of the conclusions obtained by the linear analysis. This was done using the method of characteristics in a similar way to that proposed by Crowley *et al.* (1992). Unlike other finite-difference schemes, which usually distort the shape of the waves and introduce unreal artificial decay of waves, resulting from numerical dissipation, the method of characteristics is able to simulate accurately wave propagation and evolution. However, the method of characteristics cannot be applied directly to [1]–[5], since the system is not strictly hyperbolic as some characteristics have infinite velocity (also for $\sigma = 0$). Therefore, the method was applied to a somewhat simplified transient form, which assumes that the gas velocity is much larger than the liquid velocity and the dynamic response of the gas variables is very quick, such that the gas can be assumed to be in a quasi-steady-state condition. These approximations lead to the following equations:

$$\frac{\partial h_L}{\partial t} + U_L \frac{\partial h_L}{\partial x} + \frac{A_L}{A'_L} \frac{\partial U_L}{\partial x} = 0, \qquad [29]$$

$$A_G U_G = A U_{GS}, \qquad [30]$$

$$\rho_L \left(\frac{\partial U_L}{\partial t} + U_L \frac{\partial U_L}{\partial x} + g \cos\beta \frac{\partial h_L}{\partial x} \right) = -\frac{\partial P_{iL}}{\partial x} - \frac{\tau_L S_L}{A_L} + \frac{\tau_i S_i}{A_L} - \rho_L g \sin\beta \qquad [31]$$

and

$$\rho_G \left(U_G \frac{\partial U_G}{\partial x} + g \cos\beta \frac{\partial h_L}{\partial x} \right) = -\frac{\partial P_{iG}}{\partial x} - \frac{\tau_G S_G}{A_G} - \frac{\tau_i S_i}{A_G} - \rho_G g \sin\beta. \qquad [32]$$

Eliminating the pressure drop from [31] and [32], and using [30], yields

$$G\frac{\partial h_L}{\partial x}+\frac{\partial U_L}{\partial t}+U_L\frac{\partial U_L}{\partial x}-\frac{\sigma}{\rho_L}\frac{\partial^3 h_L}{\partial x^3}+E=0, \qquad [33]$$

where

$$G=\frac{(\rho_L-\rho_G)g\cos\beta}{\rho_L}-\frac{\rho_G A^2 U_{GS}^2 A_L'}{\rho_L A_G^3} \qquad [34]$$

and

$$E=-\frac{F}{\rho_L}, \qquad [35]$$

where F is given by [9].

A KH linear stability analysis on the simplified equations [29] and [33] yields the following stability criterion:

$$\left[\frac{\left(-\frac{\partial F}{\partial R_L}\right)_{U_{LS}}}{\left(\frac{\partial F}{\partial U_{LS}}\right)_{R_L}}-U_L\right]^2+\frac{\rho_G U_{GS}^2 R_L}{\rho_L R_G^3}-\frac{g\cos\beta(\rho_L-\rho_G)\frac{A}{A_L'}R_L}{\rho_L}-\frac{\sigma}{\rho_L}\frac{A}{A_L'}R_L k^4<0. \qquad [36]$$

Figure 10 compares the results of the neutral stability curves for the VKH and IKH analyses as obtained by using the accurate formulation [1]–[4] and the simplified formulation [29, 33]. It can be seen clearly that the neutral stability curves of the simplified formulation are very close to the accurate ones for horizontal, upward and downward inclinations. In addition, the simplified formulation succeeds in predicting the behavior of the amplification factor correctly. As for the exact analysis, the region between the VKH and IKH neutral stability curves, on the U_{LS}–U_{GS} map, is a region of low amplification factors, while the region outside the IKH neutral stability curve is a region of very large amplifications. Since the two approaches (the accurate formulation and the simplified one) yield essentially the same results for the neutral stability curves and for the

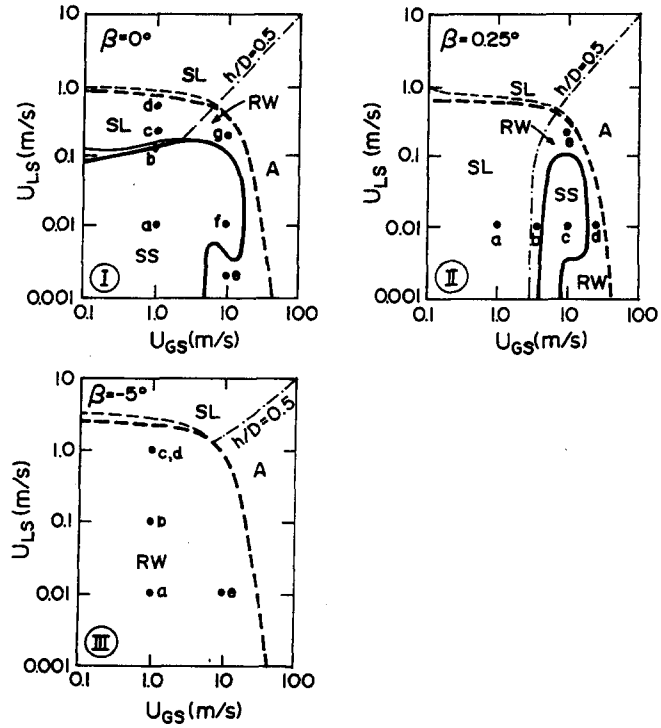

Figure 10. Flow pattern boundaries by the IKH and the VKH analyses. Air–water, 5 cm dia, atmospheric pressure, 25°C. ——, VKH (simplified); ——, VKH (exact); – – – –, IKH (simplified); – – – –, IKH (exact); SS—stable stratified; RW—roll waves; SL—slug; A—annular.

amplification factor by the linear analysis, it would be safe to use the simplified approach also for the investigation of the transient behavior.

In addition, the surface tension is neglected ($\sigma = 0$). This is a very reasonable approximation, since we are interested only in long-wave phenomena for which the surface tension is negligible anyway. Note, that the surface tension has no effect on the neutral stability criterion since the criterion should apply to all wavelengths and the instability condition for the long waves is the same as the instability condition for $\sigma = 0$ ([18] and [36]). Thus, zero surface tension is a valid physical approximation.

The hyperbolicity of formulation [29, 33] with $\sigma = 0$ was checked and the velocities of the characteristics were found:

$$C_H = U_L + \sqrt{GH_L} \quad [37]$$

and

$$C_L = U_L - \sqrt{GH_L}; \quad [38]$$

C_H is the characteristic with high velocity, while C_L is the slower characteristic. C_L can either be positive or negative; it is negative for subcritical flow and positive for supercritical flow. H_L is the pseudo liquid level ($H_L = A_L/A'_L$).

When $G < 0$ the characteristic velocities become imaginary and the system is ill-posed. Note, that the condition of $G < 0$ for the equilibrium level is identical to the stability criterion for the inviscid case (for $\sigma = 0$). Thus, our transient simulation is limited to the zone bounded by the IKH neutral stability curve, which is, actually the zone we are interested in. There is no question as to the zone outside the IKH neutral stability curve, as this is a region where any infinitesimal disturbance will grow exponentially. This can be seen from the very high rate of amplification (Barnea & Taitel 1993) as well as on physical grounds, since in this zone the suction generated over the wave crest due to the Bernoulli effect overcomes the stabilizing effect of gravity. This effect is in phase with the wave height and accelerates with wave growth. Hence, in this region we will always observe the transition from stratified flow to either slug flow, in the case of high liquid holdup, or annular flow, in the case of low liquid holdup. On the other hand, the region below the IKH curve is a region of either stable steady-state solutions or unstable solutions, but with low amplification rate (based on the linear analysis). The behavior in the non-linear range was not clear and it was speculated on the basis of the linear analysis. We shall now examine the dynamic evolution of the wave (growth or decay), using dynamic simulations.

Applying the method of characteristics, [29] and [33] with $\sigma = 0$ are converted into two ordinary differential equations along two characteristic directions as follows:

$$\frac{dh_L}{dt} - B\frac{dU_L}{dt} - BE = 0 \quad \text{along} \quad \frac{dx}{dt} = C_L \quad [39]$$

and

$$\frac{dh_L}{dt} + B\frac{dU_L}{dt} + BE = 0 \quad \text{along} \quad \frac{dx}{dt} = C_H, \quad [40]$$

where

$$B = \sqrt{\frac{H_L}{G}}. \quad [41]$$

Equations [39] and [40] were solved numerically. The simulation procedure starts with the equilibrium initial conditions, upon which a finite disturbance in the form of a solitary wave is imposed. The inlet conditions are given at $x = 0$, while the downstream conditions extend to infinity. For supercritical flow ($C_L > 0$), the inlet condition at $x = 0$ is given by the aforementioned equilibrium condition and, since the waves propagate only downstream, it never reaches the entrance at $x = 0$. For subcritical flow ($C_L < 0$), the wave that propagates upstream is reflected at the entrance, such that the conditions of constant known flow rate (U_{LS}) and the differential equation along the negative characteristic (C_L) are satisfied at $x = 0$.

The propagation of the wave is illustrated in figures 11 and 12. In these figures the liquid level along the pipe is plotted for successive steps of the calculations. The lowest curve corresponds to

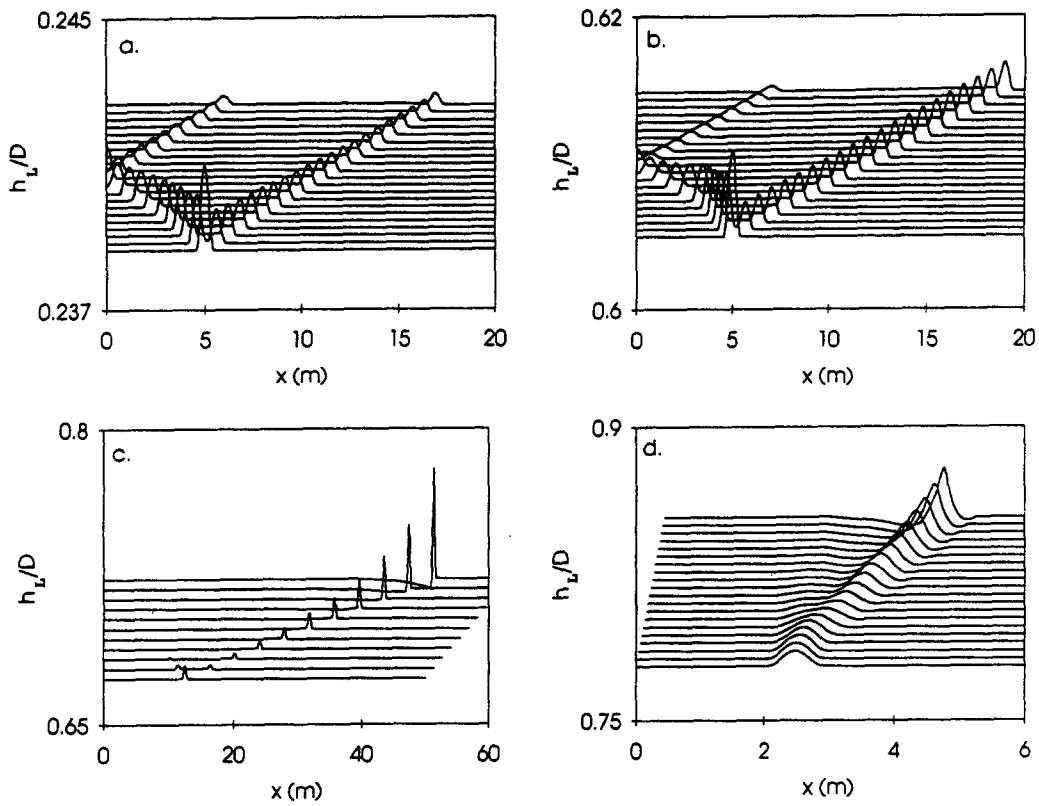

Figure 11. Evolution of a finite disturbance. Horizontal, air–water, 5 cm dia. (a) $U_{LS} = 0.01$ m/s, $U_{GS} = 1$ m/s, stable-wave decays; (b) $U_{LS} = 0.12$ m/s, $U_{GS} = 1$ m/s, neutral stability; (c) $U_{LS} = 0.2$ m/s, $U_{GS} = 1$ m/s, growth—unbounded growth; (d) $U_{LS} = 0.5$ m/s, $U_{GS} = 1$ m/s, growth—unbounded growth.

the initial conditions and the values of the ordinates for h_L/D apply only to this curve. The other curves show the shape of the interface as it changes with time.

Figure 11 shows the dynamic behavior for horizontal flow along a constant gas flow rate ($U_{GS} = 1$ m/s) and for increasing liquid flow rates [figures 11(a–d) correspond to the points "a" to "d" in figure 10(I)]. In figure 11(a) the liquid flow rate is relatively low ($U_{LS} = 0.01$ m/s), for which the steady-state solution is linearly stable via the VKH analysis [figure 10(I) point "a"]. This steady state is also stable to finite disturbances, as observed by the decay of the waves' amplitude. This case is an example of a subcritical case, where the initial solitary wave splits into two waves that propagate upstream and downstream. Both decay with time. The wave that moves to the left is reflected at the pipe entrance and continues to move in the downstream direction. All the steady-state points that are bounded within the VKH neutral stability curve, i.e. that are linearly stable, were found to be stable also to finite disturbances.

Figure 11(b) is an example for the case of marginal stability, located exactly on the VKH neutral stability curve. As can be seen, the waves propagate eventually without any change in their amplitude.

Figures 11(c) and (d) are examples of steady states that lie in the region between the VKH and IKH neutral stability curves. Namely, these steady states are unstable for the VKH analysis but are stable for the IKH analysis. This region was previously found, by linear analysis (Barnea & Taitel 1993), to be a region of low amplification rate and was interpreted as a wavy region that will undergo transition to slug flow only for high liquid levels. The non-linear simulation allows a better insight into the evolution beyond the linear range. Figures 11(c) and (d) demonstrate how the waves grow with time. Figure 11(c) shows the behavior for the case of subcritical flow, while figure 11(d) demonstrates the case of supercritical flow. In both cases the "left" wave decays quite rapidly, while the "right" wave grows until it reaches a condition for which G over the wave crest [34] becomes negative. When G is negative the equations become ill-posed, since the characteristics at the wave crest become imaginary and the method of characteristics fails. Physically, ill-posedness

is associated with instability of infinite amplification rate at the limit of the short wavelength (Ramshaw & Trapp 1978), which is a sufficient mathematical condition for the absence of a solution. Nevertheless, the physical interpretation of this condition is that when the amplitude of the wave reaches the condition of $G < 0$, it means that the suction generated over the wave crest due to the Bernoulli effect overcomes the stabilizing influence of gravity. This effect is in phase with the wave height, hence, once this condition is reached, the wave will grow unboundedly. Our interpretation is that when this situation occurs, transition from stratified flow will occur. For low void fraction ($h_D/D > 0.5$), transition to slug flow will take place; while transition to annular flow will take place for high void fraction ($h_L/D < 0.5$). Thus, figures 11(c) and (d) represent the conditions of transition to slug flow.

Note that beyond the IKH neutral stability line, the condition of $G < 0$ is satisfied for the equilibrium liquid level. For $h_L/D > 0.5$, slug flow will result; while for $h_L/D < 0.5$, annular flow is obtained. In the region below the IKH and above the VKH neutral stability lines, this condition of $G < 0$ is achieved locally over the wave crest in the process of wave growth. It is interesting to note that this local condition occurs only within the region of high equilibrium liquid level ($h_L/D > 0.5$). This suggests that annular flow does not take place within the region bounded by the IKH and VKH neutral stability lines. This is consistent with the conclusions based on the linear analysis.

Figure 12 demonstrates the dynamic response of the system at higher gas flow rate, where the film thickness is quite thin [along the line e–g in figure 10(I)]. Figure 12(f) corresponds to a stable condition. It clearly demonstrates that a finite wave decays, the amplitude decreases and the wave shape flattens while propagating downstream.

Figures 12(e) and (g), on the other hand, correspond to steady states that are unstable by the VKH analysis and stable by the IKH analysis. In these cases the waves grow and, at the same time, they are distorted to the point that they become multivalued (multiple values of h_L for the same

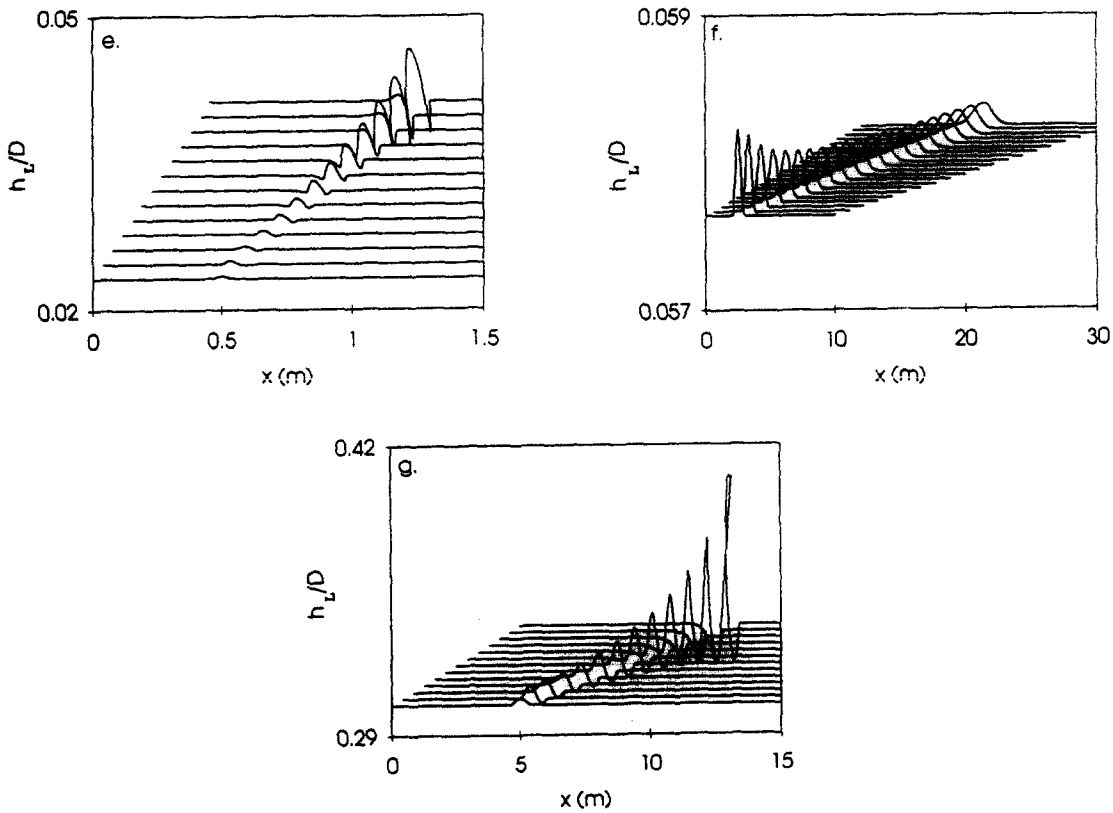

Figure 12. Evolution of a finite disturbance. Horizontal, air–water, 5 cm dia. (e) $U_{LS} = 0.002$ m/s, $U_{GS} = 10$ m/s, growth—leading to wave break; (f) $U_{LS} = 0.01$ m/s, $U_{GS} = 10$ m/s, stable-wave decays; (g) $U_{LS} = 0.2$ m/s, $U_{GS} = 10$ m/s, growth—leading to wave break.

value of x). This condition is interpreted as a wave break, which means that the waves will not continue to grow and the interface will remain wavy. This is consistent with the previous interpretation for this region, which was based solely on the linear stability analysis (Barnea 1991a; Barnea & Taitel 1993). Bruno & McCready (1988) also suggested that solitary waves which begin to break generate into roll waves. Note that all cases shown in figure 12 are for a supercritical situation with two positive characteristic velocities that have fairly close values.

The behavior of the waves for the case of upward inclined flow was checked along a constant liquid flow rate [points "a"–"d" in figure 10(II)] and along a constant gas flow rate (points "c" and "e"). The simulations of the waves' evolution are detailed in Barnea & Taitel (1994). It was found that within the bell-shaped neutral stability curve all the disturbances decay. For points "b", "d" and "e", which are unstable by the VKH analysis and stable by the IKH analysis, for which $h_L/D < 0.5$, the waves grow up to a multivalued solution, i.e. up to wave break, and the region is a region of roll waves. Point "a" is typical of solutions that are unstable by the VKH analysis and stable by the IKH analysis, for which $h_L/D > 0.5$. These solutions are in the slug flow regime. The non-linear simulation shows that waves in this region grow and reach the point where the condition $G < 0$ is obtained over the wave crest.

For downward flow [figure 10(III)] the whole region below the IKH neutral stability curve is unstable by the VKH analysis. The numerical simulation shows that wave break is always reached in this region (Barnea & Taitel 1994). This result is somewhat different from the previous conclusions that were based on the linear analysis. According to the linear analysis interpretation, solutions that are unstable by the VKH analysis and stable by the IKH analysis, for which $h_L/D > 0.5$, are in slug flow. The non-linear analysis suggests that only waves that reach the condition of $G < 0$ at the crest and for which $h_L/D > 0.5$ are in slug flow, whereas breaking waves on a liquid film of $h_L/D > 0.5$ stay wavy. Note that the agreement of this result with experimental results is better for downward flow [see figure 7 in Barnea (1991a)]. For the case of horizontal and upward inclined flow, growing waves that reach the condition of $G < 0$ lie approximately, in the region of $h_L/D > 0.5$, while growing waves that break are in the region of $h_L/D < 0.5$.

Comparison with Experimental Results

The interfacial stability analysis of stratified flow is applied to the prediction of transition from stratified flow. Solutions that are unstable by the IKH analysis are solutions for which the Bernoulli amplification overcomes the stabilizing effect of gravity, at the steady-state condition. These solutions are characterized by a very high amplification rate, resulting in the transition to slug flow, for high liquid holdup ($h_L/D > 0.5$), and to annular flow, for low liquid holdup ($h_L/D < 0.5$). On the other hand, solutions that are unstable by the VKH analysis and stable by the IKH analysis are solutions with a low amplification factor. It was suggested that this instability results in a wavy interface (roll waves) and only for high liquid level ($h_L/D > 0.5$) will the wave block the pipe, causing transition to slug flow.

Based on the above, a combined model which uses the VKH and IKH analyses has been suggested for the prediction of the flow pattern transition:

- The neutral stability condition obtained by the VKH analysis demarcates between stable stratified flow (stratified smooth or small amplitude waves) and unstable flow. The latter is either slug flow, annular flow or large-amplitude roll waves.
- Within the unstable region, the line of $h_L/D = 0.5$ demarcates between slug flow and annular or roll waves.
- In the unstable high void region $h_L/D < 0.5$, the neutral stability condition of the IKH analysis demarcates between roll waves and annular flow.

The results of the non-linear simulation confirm most of the linear analysis results and supports the previous interpretation regarding the flow pattern transition. Within the region bounded between the VKH and IKH neutral stability curves, two typical developments of the growing wave are identified: (a) the wave grows and reaches a point where $G < 0$ at the wave crest; and (b) the wave grows and reaches a point of multiple values. When the condition of $G < 0$ occurs in the growing process of the wave, the wave will continue to grow unboundedly and if the equilibrium

liquid level is above $h_L/D = 0.5$ slug flow will result, otherwise the flow is annular. When a multiple-valued profile is obtained in the growing process of the wave it is interpreted as a wave break, which causes a wavy interface. For horizontal and upward inclined flow the condition of wave break takes place at $h_L/D < 0.5$, while the growing wave that reaches the condition $G < 0$ lies approximately in the region of $h_L/D > 0.5$. So far these conclusions are consistent with the results of the linear stability analysis. For downward inclined flow it was found that the condition of wave break (in the region that is unstable by the VKH analysis and stable by the IKH analysis) takes place also for $h_L/D > 0.5$. This result slightly changes the location of the transition boundary obtained by the linear analysis.

Figure 13 demonstrates the effect of pipe inclination and liquid viscosity on the flow pattern transitions as predicted by the VKH and IKH analyses. These results are compared with the simpler Taitel & Dukler (1976) model and with available experimental data (Shoham 1982). For the case of low viscosities ($\mu_L = 1$ cP), the Taitel & Dukler prediction is quite similar to the results of the present model for the flow pattern transition in horizontal, upward and downward inclinations. Note, however, that the region bounded between the IKH and VKH neutral stability curves considered here as a region of stratified flow with large-amplitude waves, while Taitel & Dukler designate this region, at high liquid flow rates, as wavy-annular [Nicholson *et al.* (1978) called this region proto-slug and Lin & Hanratty (1987) called it pseudo-slug]. For higher viscosities, the Taitel & Dukler (1976) model underpredicts the transition boundary from stratified flow for horizontal and upward inclined flows. For downward flow, on the other hand, the Taitel & Dukler transition boundary from stratified flow is very close to the present prediction.

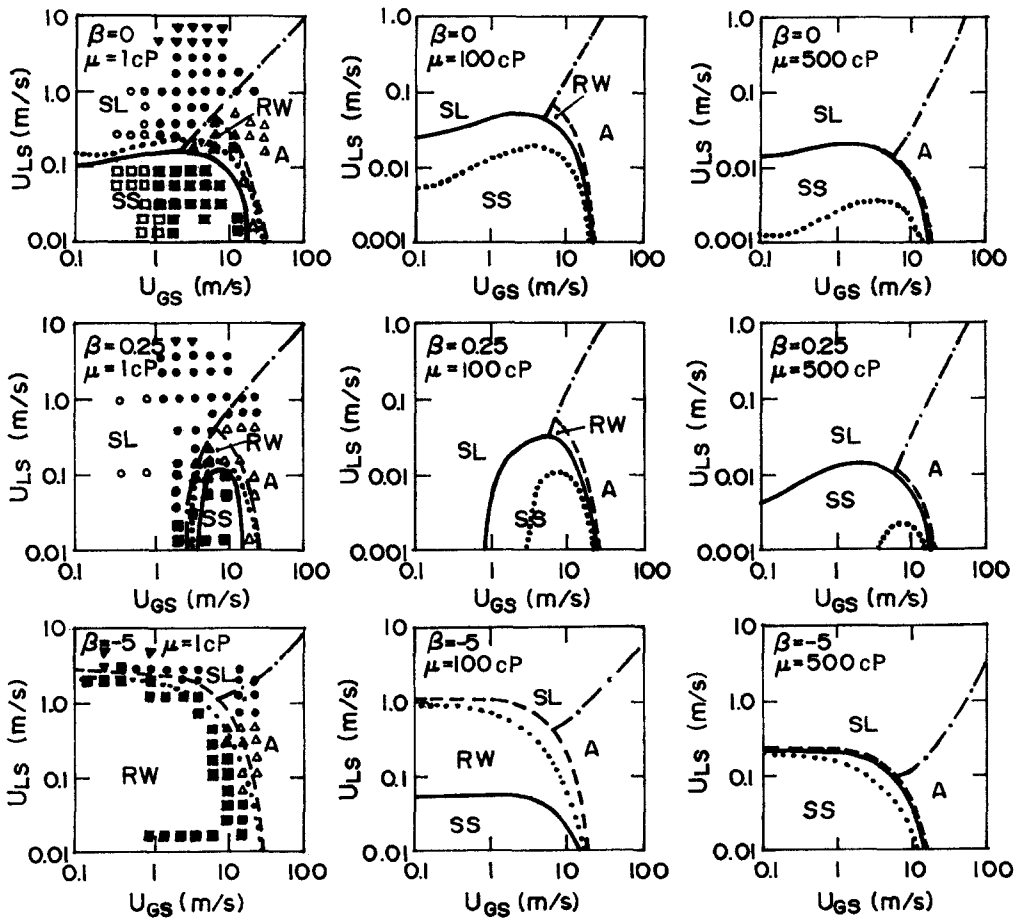

Figure 13. Transition from stratified flow. ——, VKH; – – –, IKH; · · · · · · , Taitel & Dukler (1976) —·—·—, $h_L/D = 0.5$. Data (Shoham 1982): □, stratified smooth; ■, stratified wavy; ▲, wavy annular; ○, elongated bubble; ●, slug; △, annular.

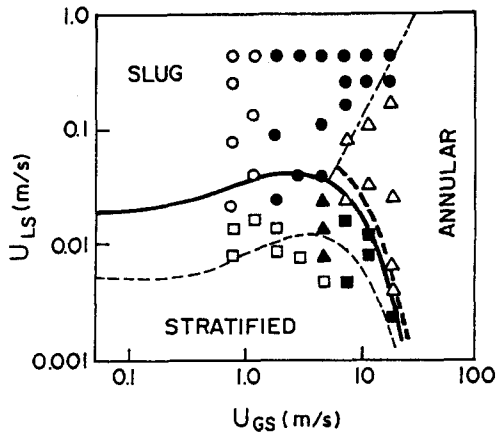

Figure 14. Flow pattern data of Taitel & Dukler (1987) for 90 cP glycerol/water–air. Horizontal, 3.8 cm dia pipe. Comparison with the present model and the Taitel & Dukler (1976) model. □, Stratified—smooth; ■, stratified—wavy; ○, elongated bubbles; ●, slug; △, annular; ▲, wavy—annular; ——, VKH theory; – – –, IKH theory; – – – –, $h_L/D = 0.5$; – – – –, Taitel & Dukler (1976).

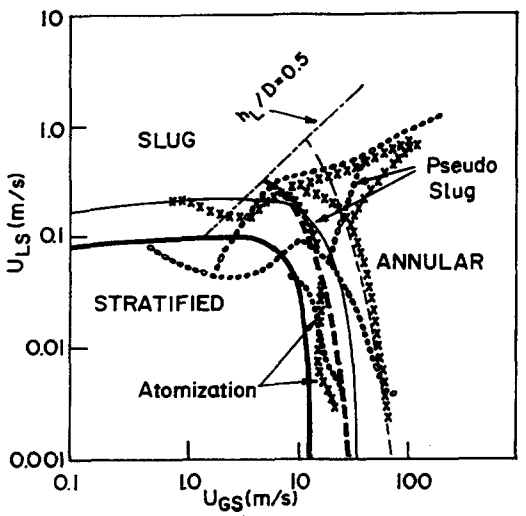

Figure 16. Effect of pipe diameter on the flow pattern. Air–water, atmospheric pressure, horizontal pipe. VKH, ——, IKH, – – – –}$D = 0.0254$ m; VKH, ——, IKH, – – – –}$D = 0.0953$; Data of Lin & Hanratty (1987), ○○○○○, $D = 0.0254$; × × × × ×, $D = 0.0953$.

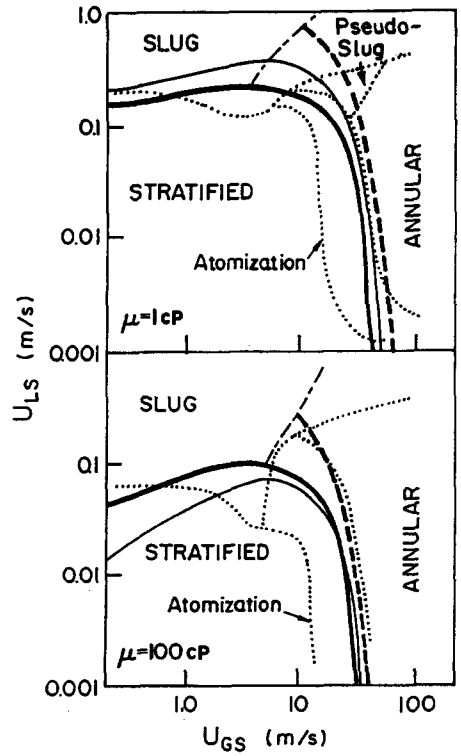

Figure 15. Flow patterns data of Andritsos *et al.* (1989) for 1 and 100 cP glycerol/water–air. Horizontal, 9.53 cm dia pipe. Comparison with the present model and the Taitel & Dukler (1976) model. ——, VKH theory; – – –, IKH theory; · · · · · ·, Andritsos *et al.* (1989); – – – –, $h_L/D = 0.5$; ——, Taitel & Dukler (1976).

Figure 14 is a plot of the flow pattern data obtained by Taitel & Dukler (1987) for 90 cP glycerol/water–air in a horizontal 3.8 cm dia pipe. It can be seen that the present model predicts the experimental results better than the Taitel & Dukler (1976) criterion.

Figure 15 presents the experimental transition boundaries obtained by Andritsos *et al.* (1989) for a 9.53 cm dia pipe with liquid viscosities of 1 and 100 cP. These data are compared with the present model and with the Taitel & Dukler (1976) model. The effect of viscosity on the transition to slug flow is well-predicted by the present model; higher viscosities cause transition at lower liquid velocities. Again, the Taitel & Dukler model slightly underpredicts the results at high liquid viscosity. The region bounded between the VKH neutral stability curve, the IKH neutral stability curve and $h_L/D = 0.5$, for high liquid flow rates, predicts quite well the pseudo-slug region. However, it does not seem to cover the whole range between atomization and annular flow, as given by the Andritsos *et al.* (1989) data.

Figure 16 presents the experimental results obtained by Lin & Hanratty (1987) for the effect of pipe diameter on the stability of stratified flow. The effect of pipe diameter on the transition from stratified to slug and annular flows, obtained in the calculations, is reasonably confirmed by the experimental results. On the other hand, the experimental results do not support the influence of the pipe diameter on the wavy to annular transition at very low liquid flow rates.

STRUCTURAL STABILITY

Annular Flow

So far we have discussed only the KH interfacial instability. This is not sufficient to determine the stability of separated flows.

For the case of annular flow, for example, the steady-state solutions are always unstable, owing to the KH type of instability, since the stabilizing influence of gravity is either absent (for vertical flow) or negligible (see [18]). The physical interpretation of this instability is that steady annular flow is dynamically unstable with respect to its interface, always resulting in a wavy interface. The question of interest, in this case, is whether this kind of steady annular flow is a stable structure with respect to its average film thickness, which is obtained for the steady state using an effective interfacial shear stress. In addition, for the case of upward (inclined and vertical) cocurrent and countercurrent annular flow, multiple steady-state solutions may exist (Barnea & Taitel 1989). In this case one may question whether multiple holdup values exist in stable annular flow.

In order to answer these questions, Barnea & Taitel (1990) suggested that the interfacial instability which exists inherently in annular flow, is ignored and that the stability of the structure is checked by a formulation where a uniform film thickness along the pipe is assumed, resulting in the following transient momentum and continuity equations for the liquid:

$$\frac{dU_L}{dt} = -\frac{U_{LS}}{R_L l}\left(U_L - \frac{U_{LS}}{R_L}\right) + \frac{F}{\rho_L} \qquad [42]$$

and

$$\frac{dR_L}{dt} = \frac{1}{l}(U_{LS} - U_L R_L), \qquad [43]$$

where F is given by [9] with $S_G = 0$ and $g = 0$ for annular flow (l is the pipe length).

For the case of annular flow, where $U_G \gg U_L$, it is convenient to present F in the following form:

$$F = \frac{S_i}{A}\left(\frac{1}{R_L} + \frac{1}{R_G}\right)(\tau_i - \tau_{iL}); \qquad [44]$$

τ_{iL} is the interfacial shear stress needed to maintain a steady-state flow for a given liquid velocity, U_L, and film thickness, δ,

$$\tau_{iL} = \frac{(\rho_L - \rho_G)Ag \sin\beta + \dfrac{\tau_L S_L}{R_L}}{S_i\left(\dfrac{1}{R_L} + \dfrac{1}{R_G}\right)}, \qquad [45]$$

and τ_i is the shear stress provided by the gas, which depends on the gas velocity, U_G, and the film thickness δ,

$$\tau_i = \tfrac{1}{2} f_i \rho_G U_G^2. \qquad [46]$$

For steady state $\tau_{iL} = \tau_i$.

A linear stability analysis on the above two ordinary differential equations, [42] and [43], yields the following criterion for the structural stability of cocurrent stratified flow:

$$\left(\frac{\partial F}{\partial R_L}\right)_{U_{LS}, U_{GS}} > 0 \qquad [47]$$

or

$$\left.\frac{\partial \tau_{iL}}{\partial R_L}\right|_{U_{LS}} - \left.\frac{\partial \tau_i}{\partial R_L}\right|_{U_{GS}} < 0. \qquad [48]$$

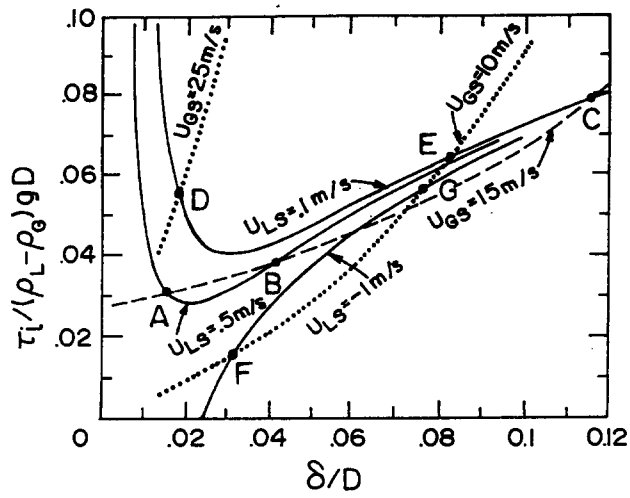

Figure 17. Steady-state solutions and stability diagram for vertical annular flow. Air–water, atmospheric pressure, 2.5 cm dia. ——, τ_i [45]; – – – –, τ_i [46], $f_i = 0.05$; · · · · · ·, τ_i [46], $f_i = 0.005(1 + 300\delta/D)$.

For the case of countercurrent flow, where U_{LS} is negative, a similar derivation yields:

$$\left.\frac{\partial \tau_{iL}}{\partial R_L}\right|_{U_{LS}} - \left.\frac{\partial \tau_i}{\partial R_L}\right|_{U_{GS}} > 0. \qquad [49]$$

Equations [48] and [49] provide simple and general criteria for determining the structural linear stability of the steady-state solutions. Note again, that these criteria indicate whether the steady-state solution is a stable structure with respect to its average film thickness. These criteria are easily applied by using steady-state diagrams, where τ_{iL} and τ_i are plotted vs δ/D. Figure 17 is an example of such a diagram for vertical cocurrent and countercurrent annular flows. For the case of countercurrent flow, two steady-state solutions may exist for any given pair of U_{LS} and U_{GS} values. The solution F, which corresponds to the thinner film, is stable, while solution G is unstable. For the case of cocurrent flow, two different correlations for the interfacial shear stresses, τ_i, are used. When a constant value of the interfacial friction factor, f_i, is used, multiple solutions may occur: two linearly stable solutions (points A and C) and one unstable solution (point B). When Wallis's (1969) correlation is used for f_i, a single linearly stable solution is obtained for all gas and liquid flow rates (point D for E).

Solutions E and C, which correspond to thick films, were not detected experimentally, though they were found to be linearly stable with respect to the structure. Therefore, the non-linear stability of these solutions was checked, using the same dynamic formulation [42, 43].

The non-linear stability was studied by examining the system response to finite disturbances. Numerical runs were carried out by starting the dynamic simulation at different points. The results for the case of countercurrent flow are shown in figure 18(d). It is clearly seen that the trajectories are attracted to the stable steady-state solution (point F) and repelled from the unstable solution (point G). There is a wide region of attraction towards F to the "left" of G, whereas most of the region to the "right" of point G is a "runaway" zone. Thus, counter current solutions that are linearly stable, are also stable to finite disturbances.

For the case of cocurrent flow, a single steady-state solution is obtained when Wallis's (1969) correlation is used for f_i (solutions D and E in figure 17). The two solutions were found to be linearly stable. However, finite disturbances adjacent to these steady states indicate that the solution which corresponds to the thin film (along the branch to the left of the minimum of the τ_{iL} vs δ curve in figure 17) is indeed a stable steady state that attracts the trajectories [figure 18(a)]. The solution which corresponds to the thicker film is of a peculiar character. It resembles the behavior of a stable focus in the vicinity of the steady solution. But, one can observe that this solution is unstable to finite disturbances. As shown [figure 18(b)], a finite decrease in the film thickness leads to negative film velocities, resulting in the destruction of cocurrent flow. Thus, the solutions along the branch to the right of the minimum are practically unstable.

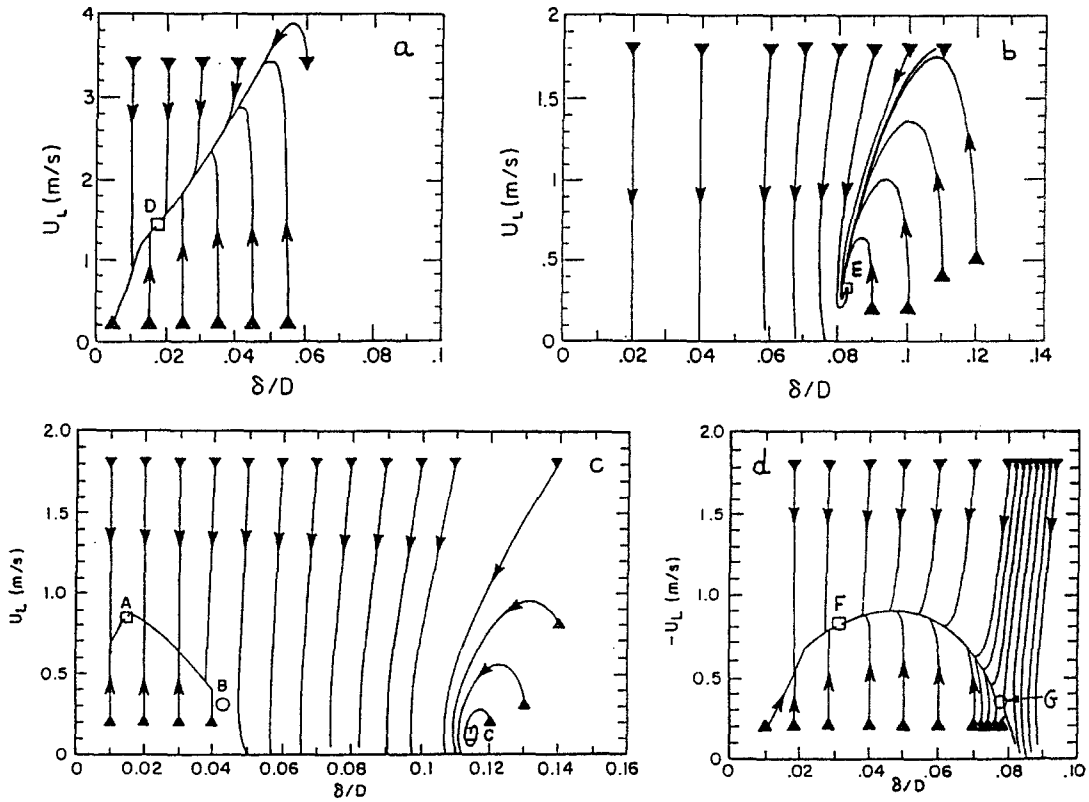

Figure 18. Dynamic simulation for the steady-state solutions shown in figure 17. □, Linearly stable steady state; ○, unstable steady state.

An interesting case is the one of cocurrent flow with a constant interfacial shear stress coefficient ($f_i = 0.05$). Figure 17 shows that in this case one can obtain three steady-state solutions—A, B and C. According to the linear analysis, A and C are stable solutions, whereas B is unstable. Figure 18(c) shows the dynamic simulations for this case. As shown, point A is a stable steady-state that attracts the trajectories, whereas B is clearly a strong repellent point. The steady-state C, however, attracts only those trajectories that are adjacent to it. Its characteristic behavior is similar to that of point E, shown in figure 18(b), which was discussed above. That is, in this case also, any finite disturbance will cause the solution to "run away". This suggests that practically this is an unstable steady state that is not likely to occur. Thus, out of the three steady-state solutions, we expect only the steady-state solution that corresponds to the thinnest film thickness to exist (point A).

Barnea (1991b) showed also that a discrete representation of the two-fluid model equations leads to the same results for the structural stability as those obtained by the uniform film analysis, provided the advective terms are approximated by backward derivatives, i.e. when the information is allowed to travel only in the downstream direction. The case of uniform film thickness, which was used before for the structural stability analysis, is, in fact, a special case of the discrete form for which a single discretization is used.

As has been mentioned, the interface of annular flow is always wavy, owing to the interfacial instability. It is interesting to observe that if it is required that the wave velocity is in the downstream direction, i.e. C_V in [19] is positive for cocurrent flow and negative for countercurrent flow, then we obtain exactly the same criterion for the linear structural stability as presented by [47], which was derived using different considerations.

Another interesting observation is that the expression for C_V, the wave velocity at the inception of the VKH instability, is exactly the same as for the kinematic wave velocity (Wallis 1969; Wu *et al.* 1987):

$$C_k = \left.\frac{\partial U_{LS}}{\partial R_L}\right|_{U_{LS}+U_{GS}} = C_V \qquad [50]$$

Thus, in order to maintain a stable structure, it is required that the kinematic waves propagate in the downstream direction.

The KH and structural stability analyses for annular flow can be applied as a criterion for the flow pattern transition from annular flow. In steady annular flow, the interface is always unstable, owing to the KH instability. For high liquid holdup [$A_L/A = 0.24$, see Barnea (1986)], the unstable waves will block the gas core, resulting in transition to slug flow. For high voids (low liquid holdup), transition from annular flow is controlled by the structural stability analysis. For any given liquid flow rate, when the gas superficial velocity is high enough to yield steady-state solutions to the left of the minimum on the τ_i vs δ/D curve (figure 17), annular flow is a stable solution (though the interface is unstable). For low superficial gas velocities, which yield solutions to the right of the minimum, the steady-state solutions are structurally unstable and transition to intermittent flow will take place. This minimum on the τ_i vs δ/D curve is associated with the flow reversal point. For flow conditions to the right of this minimum a partial amount of liquid flows downward, accumulates at the pipe entrance and transition to intermittent flow occurs.

Thus, transition to intermittent flow will take place either when the liquid holdup is high or when the flow is structurally unstable. A complete description of the application of these mechanisms to the transition from annular flow in the whole range of pipe inclination is given by Barnea (1986). Figure 19 compares the theoretical transition boundaries with the experimental data.

Stratified Flow

The structural considerations apply also to stratified flow and it will be shown that there are cases where the flow is stable according to KH analysis but unstable structurally and therefore would not exist. Similar to the case of annular flow, the steady-state solutions for stratified flow are also not unique and multiple solutions may occur for some operating conditions in upward inclined flow (Landman 1991a, b; Barnea & Taitel 1992). In this case it is necessary to determine

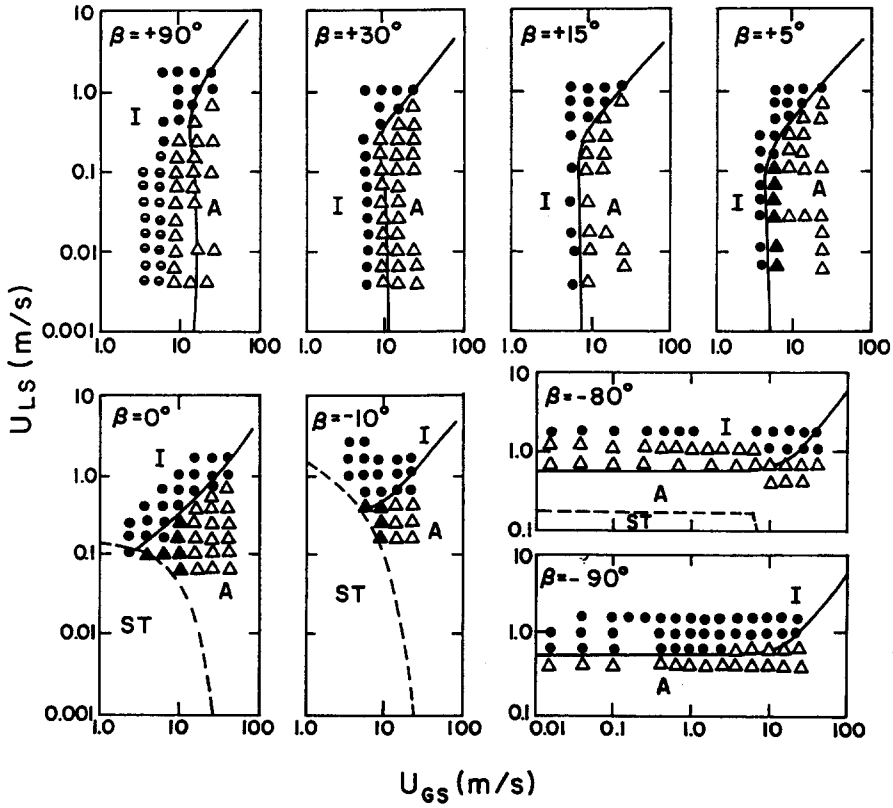

Figure 19. Annular to intermittent transition. Air–water, 0.1 MPa, 25°C, 2.5 cm dia. ——, Theory; – – – –, Taitel & Dukler (1976) model. Data of Shoham (1982). △, Annular; ▲, wavy annular (A), ●, slug; and ⊖, churn (I).

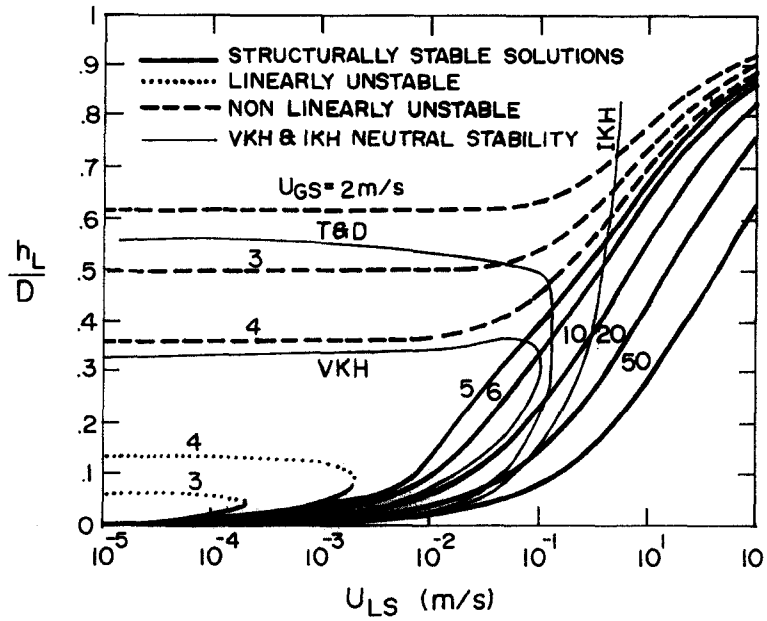

Figure 20. Multiple solutions and stability of stratified flow. Air–water, $\beta = 0.25°$, 0.1 MPa, 5.0 cm dia.

which solutions will actually exist, whether hysteresis is possible in stratified flow and what are the conditions for transition from stratified flow.

The KH analysis applied before was employed only on the first steady-state solution (when having multiple solutions) or on the single steady solution (when a single solution exists). The stability of the structure will now be examined for each of the steady-state solutions and only when the solution is structurally stable, will the KH analysis be checked further to determine whether the interface is stable and if it is not, what results from this instability.

A typical example of steady-state stratified flow solutions is shown in figure 20. In this figure the liquid level is plotted vs the liquid superficial velocity for various gas flow rates for an air–water system in a 0.25° upward inclined pipe. In this figure the region bounded by the IKH neutral stability line is a region where the flow is stable by the IKH analysis. Likewise, the region bounded by the VKH neutral stability line is a stable region by the VKH analysis.

The stability of the structure of stratified flow is examined in a similar fashion to the analysis of annular flow. The first step is to perform a linear stability analysis of the structure, [42] and [43], which results in the criterion [47]. The non-linear instability is examined by numerical simulations using the simplified transient formulation, presented by [42] and [43].

An example of such a transient numerical simulation, for the case $U_{LS} = 0.002$ m/s and $U_{GS} = 4$ m/s, is shown in figure 21, where the trajectories of the transient simulation are plotted on a phase space of U_L vs R_L. For this case, three steady-state solutions are obtained. The transient simulation starts with conditions close to the linearly unstable solution (B) ($U_L = 0.0375$ m/s and $R_L = 0.0534$). As seen, when we start at a point somewhat to the left of the unstable solution (B), we end up with the stable "thin" solution (A) ($U_L = 0.0543$ m/s and $R_L = 0.0368$). Starting at a point to the right of the unstable solution yields a trajectory that eventually ends up at the linearly stable thick solution (C) ($U_L = 0.006$ m/s and $R_L = 0.325$), but the trajectory is in the form of severe oscillations before the point of steady state is reached. We consider this third solution unstable, because the trajectory passes through negative liquid velocities. When the liquid velocity becomes negative, the structure of cocurrent flow is destroyed and transition to slug flow will ensue. This negative value of U_L is obtained also when the starting point is quite close to the third solution.

In order for a steady-state solution to be stable, it is required that all trajectories end up at this steady-state point without passing through negative liquid velocities during the dynamic response. It is not practical to determine this non-linear stability condition by checking the dynamic response of all possible disturbances. A way of solving this problem is presented by Barnea & Taitel (1992), and the results of the solutions which were found to be unstable in the non-linear sense are designated by the dashed lines in figure 20.

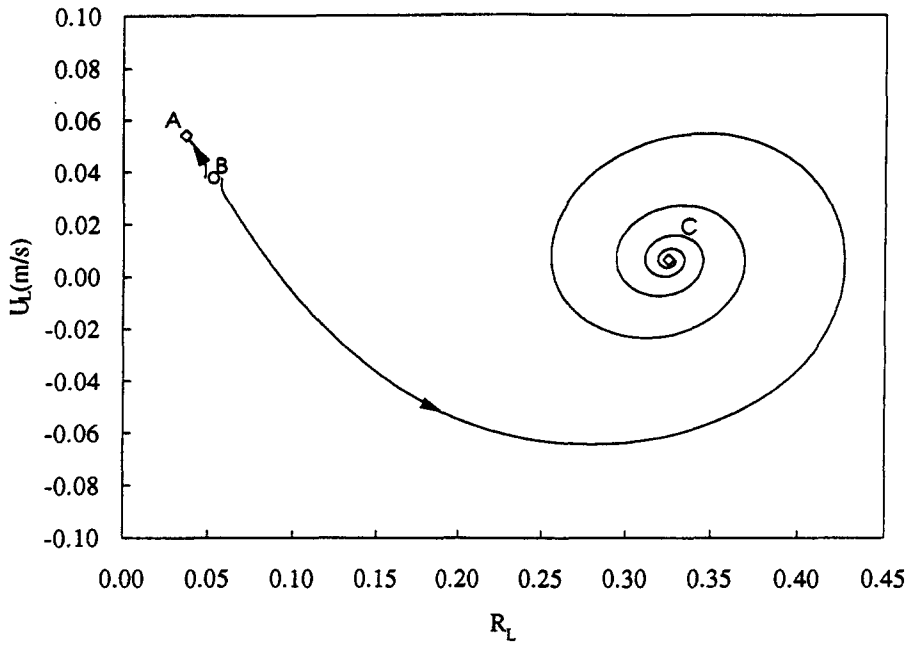

Figure 21. Dynamic simulation: non-linear structural stability. Air–water, $\beta = 0.25°$, $D = 5$ cm, $l = 1$ m, $U_{LS} = 0.002$ m/s, $U_{GS} = 4$ m/s.

In figure 20, the structurally stable solution for the liquid level are plotted as solid lines, the linearly unstable solutions as dotted lines and the non-linear unstable solutions as dashed lines. Usually, when we have three solutions the thinnest solution is structurally stable, the middle solution is linearly unstable and the thickest solution is unstable to finite disturbances. When a single solution exists, it is always linearly stable but it may be unstable to finite disturbances, as can be seen, for example, for $U_{GS} = 2$ m/s (figure 20).

The existence of stratified flow is thus determined by both the structural stability and the interfacial (KH) stability analyses. Figure 20 presents the whole story. Provided that the flow is structurally stable (the lines are solid), the region bounded by the VKH neutral stability line is in stratified smooth or stratified flow with small-amplitude waves, while the region bounded between the VKH neutral stability curve, the IKH neutral stability line and the line $h_L D = 0.5$ is a region of stratified flow with large-amplitude waves. For example, the solutions along $U_{GS} = 4$ m/s, which are bounded between the VKH, IKH and $h_L/D < 0.5$ lines, are structurally unstable and will not exist, while the solutions along $U_{GS} = 5$, 6 and 10 m/s, which are bounded in this region, are structurally stable and will result in stratified flow with high-amplitude waves.

The structural stability has been analyzed by the use of a simplified transient formulation, which assumed a uniform film thickness along the pipe during the transient changes. This is a model that aims to ignore the wavy interface and to consider only the structure. Although such a model for examining the structure makes sense, and the results obtained agree with experimental observations, it can still be subject to criticism due to the fact that the physics is too simplified. The method of characteristics, applied to the two-fluid model equations, [29–32] which was used before for the simulation of the non-linear interfacial behavior, will be used now also to observe the behavior of the structure.

As mentioned before the structural stability was helpful, in particular, in distinguishing between physical and non-physical solutions when one has multiple steady-state solutions. For example, for the case of upward flow ($\beta = 0.25°$), for $U_{LS} = 0.002$ m/s and $U_{GS} = 4$ m/s, we have three steady-state solutions, as can be seen from figure 20. The first two solutions are stable by the VKH analysis, while the third one is unstable by the VKH analysis and stable by the IKH analysis. Figure 22 demonstrates the behavior of a wave imposed on each of the three steady-state solutions. Figure 22(a) shows a wave on the first solution (the thinnest h_L/D) and, as can be seen, the waves decay. Figure 22(b) shows also that the second solution is stable by the VKH analysis and the waves also decay. The third solution is unstable by the VKH analysis and the wave grows up to the

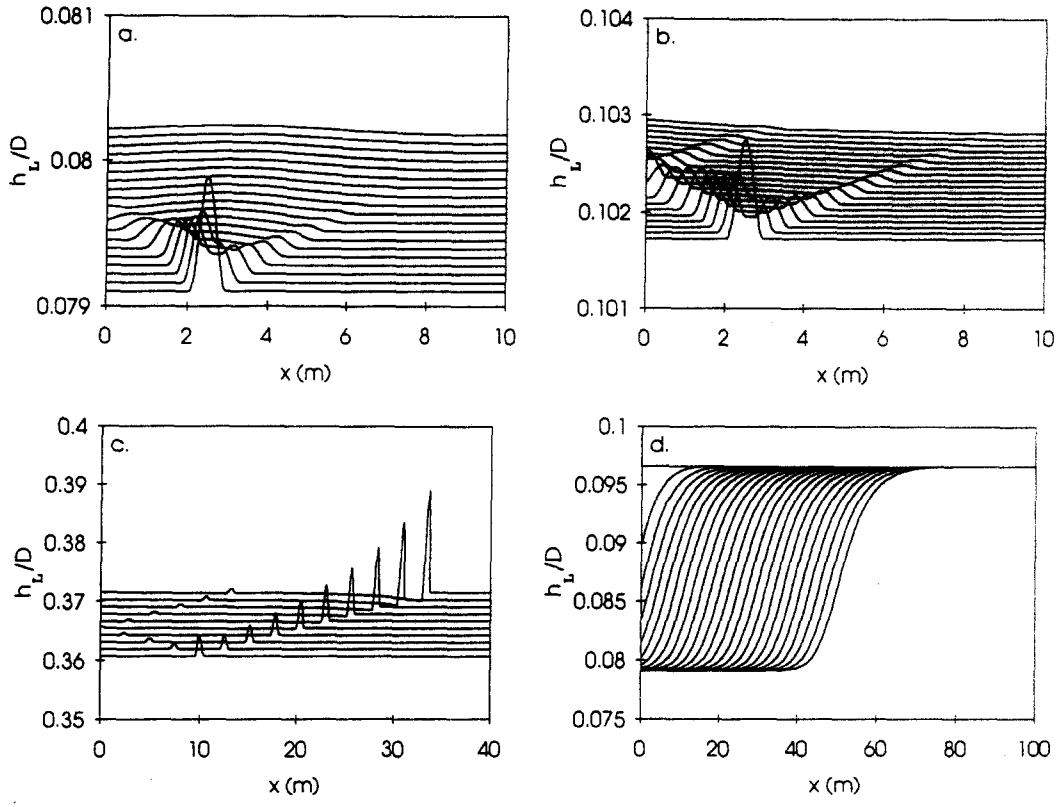

Figure 22. The case of multiple solutions. Upward flow, $\beta = 0.25°$, air–water, 5 cm dia, $U_{LS} = 0.002$ m/s, $U_{GS} = 4$ m/s. (a) First solution, $h_L/D = 0.0791$, stable to VKH; (b) second solution $h_L/D = 0.1017$, stable to VKH; (c) third solution $h_L/D = 0.3607$, unstable to VKH; (d) transient behavior: move away from the second solution to the first solution.

condition of wave break [figure 22(c)]. On the basis of the interfacial analysis alone, these three solutions are within the stratified flow regime. The first two are stable stratified (SS), while the third is stratified with roll waves (RW). According to the structural analysis, the first solution is structurally stable, the second is unstable and the third is unstable to large disturbances. These conclusions are substantiated by the use of the more exact (but elaborate) technique using the two-fluid model, [39] and [40]. For example, when we impose an initial condition which is below the second steady-state solution, it can be observed clearly that the liquid level approaches the first steady-state solution, which is stable to the structure, and departs from the second solution, which is unstable to the structure. Figure 22(d) demonstrates this fact. In this figure a uniform initial liquid level, somewhat less than the second steady-state solution, is imposed. The time evolution profile of the liquid level runs away from the second steady-state solution and approaches the first steady-state solution. Note that unlike figures 22(a–c), where the values of the ordinate apply only to the first profile, in figure 22(d) the ordinate is common to all the time-dependent profiles. Note also in figure 22(b), where the initial condition is a solitary wave imposed on the second steady-state solution which is structurally unstable (and stable to the interface), the wave indeed decays but the level at the entrance begins to deviate from this steady-state solution. However, the time scale for the wave decay is much shorter than the time needed to see a real change in the film thickness.

SUMMARY AND CONCLUSIONS

The transition from separated flow is considered using long-wave analysis (one-dimensional). The stability of the steady-state solutions is considered by using two types of instability: (1) the interfacial stability analysis, which indicates whether the interface is stable; and (2) the structural stability analysis, which determines if the solution is stable with respect to the average film thickness as obtained by the steady-state solutions, even if the interface is unstable.

One-dimensional KH analysis is used for analyzing the stability of the interface. Two kinds of KH analyses have been used: the inviscid analysis (IKH), in which the effect of the shear stress on the stability is neglected; and the viscous analysis (VKH), in which the shear stresses are considered. The neutral stability condition for the VKH analysis predicts the formation of an unstable interface with large-amplitude waves, while the IKH analysis is associated with the unbounded growth of the unstable waves. This interpretation is confirmed by observing the rate of amplification for both approaches. The two KH analyses have been used to predict the transition from stable stratified flow to either large-amplitude roll waves, slug flow or annular flow, depending on the type of instability and the liquid holdup of the steady-state solution.

The non-linear stability analysis of the interface is carried out using a numerical simulation which examines the system response to finite disturbances of the interface. The non-linear simulation usually confirms the conclusions based on the linear considerations. It is shown that when the interface is linearly stable, the simulation shows that waves decay with time. When the interface is unstable by the VKH analysis, the waves grow and reach a point where $G < 0$ at the wave crest or reach a point of multivalued amplitude. The condition of $G < 0$ is associated with an unbounded growth and transition to slug or annular flow (depending on h_L/D). This is also a point where the equations become ill-posed and cannot be solved by the method of characteristics. The condition of multivalued amplitude is interpreted as a wave break and it is believed to indicate a pattern of roll waves.

The interfacial stability analysis is not sufficient to determine the validity of the steady-state solutions in separated flow. The stability of the structure of separated flow should be considered in addition to the KH interfacial stability. The structural stability of annular and stratified flows was examined for infinitesimal and finite disturbances. The structural and interfacial KH stability analyses yield complete information regarding the stability of the steady-state solutions and the resulting flow pattern transition that the unstable solutions undergo. The results obtained for the structural stability are based on a somewhat idealistic picture of the real physics. The interface is assumed uniform along the pipe and the detail of the wavy structure is ignored. Numerical simulations by the method of characteristics, which uses the two-fluid model equations, confirm the structural stability concept and show that the structural stability analysis is indeed a valid and useful method.

REFERENCES

ANDREUSSI, P. & PERSEN, L. N. 1987 Stratified gas–liquid flow in downwardly inclined pipes. *Int. J. Multiphase Flow* **13,** 565–575.

ANDREUSSI, P., ASALI, J. C. & HANRATTY, T. J. 1985 Initiation of roll waves in gas–liquid flows. *AIChE Jl* **31,** 119–126.

ANDRITSOS, N. & HANRATTY, T. J. 1987 Interfacial instabilities for horizontal gas–liquid flow in pipelines. *Int. J. Multiphase Flow* **13,** 583–603.

ANDRITSOS, N., WILLIAMS, L. & HANRATTY, T. J. 1989 Effect of liquid viscosity on the stratified–slug transition in horizontal pipe flow. *Int. J. Multiphase Flow* **15,** 877.

BARNEA, D. 1986 Transition from annular flow and from dispersed-bubble flow—unified models for the whole range of pipe inclination. *Int. J. Multiphase Flow* **5,** 733–744.

BARNEA, D. 1991a On the effect of viscosity on stability of stratified gas liquid flow—application to flow pattern transition at various pipe inclination. *Chem. Engng Sci.* **46,** 2123–2131.

BARNEA, D. 1991b Stability analysis of annular flow structure, using a discrete form of the "two fluid model". *Int. J. Multiphase Flow* **17,** 705–716.

BARNEA, D. & TAITEL, Y. 1989 Transient formulation modes and stability of steady state annular flow. *Chem. Engng Sci.* **44,** 325–332C.

BARNEA, D. & TAITEL, Y. 1990 Non-linear stability and dynamic simulation of annular flow. *Chem. Engng Sci.* **45,** 3367–3371.

BARNEA, D. & TAITEL, Y. 1992 Structural and interfacial stability of multiple solutions for stratified flow. *Int. J. Multiphase Flow* **18,** 821–830.

BARNEA, D. & TAITEL, Y. 1993 Kelvin–Helmholtz stability criteria for stratified flow, viscous versus non-viscous (inviscid) approaches. *Int. J. Multiphase Flow* **19,** 639–649.

BARNEA, D. & TAITEL, Y. 1994 Non-linear interfacial instability of separated flow. *Chem. Engng Sci.* **49,** 2341–2349.

BENJAMIN, T. B. 1968 Gravity currents and related phenomena. *J. Fluid Mech.* **31,** 209–248.

BRUNO, K. & MCCREADY, M. J. 1988 Origin of roll waves in horizontal gas–liquid flows. *AIChE Jl* **34,** 1431–1440.

COHEN, S. L. & HANRATTY, T. J. 1968 Effects of waves at a gas–liquid interface on a turbulent air flow. *J. Fluid Mech.* **31,** 467–469.

CROWLEY, C. J., WALLIS, G. B. & BARRY, J. J. 1992 Validation of a one-dimensional wave model for the stratified-to-slug flow regime transition, with consequences for wave growth and slug frequency. *Int. J. Multiphase Flow* **18,** 249–271.

HANRATTY, T. J. 1983 Interfacial instabilities caused by air flow over a thin liquid layer. In *Waves on Fluid Interfaces* (Edited by MEYER, R. E.), pp. 221–259. Academic Press, New York.

HANRATTY, T. J. & HERSHMAN, A. 1961 Initiation of roll waves. *AIChE Jl* **7,** 488–497.

HANRATTY, T. J. & MCCREADY, M. J. 1992 Phenomenological understanding of gas–liquid separated flows. Presented at the *3rd Int. Wkshp on Two-phase Flow Fundamentals*, London.

JEFFREYS, H. 1925 On the formation of water waves by wind *Proc. R. Soc.* **A107,** 189–206.

KORDYBAN, E. S. 1977 Some characteristics of high waves in closed channels approaching Kelvin–Helmholtz instability. *Trans. ASME Jl Fluids Engng* **99,** 339–346.

KORDYBAN, E. S. & RANOV, T. 1970 Mechanism of slug formation in horizontal two-phase flow. *J. Bas. Engng* **92,** 857–864.

LANDMAN, M. J. 1991a Hysteresis of holdup and pressure drop in simulations of two-phase stratified inclined pipe flow. In *Proc. 5th Int. Conf. on Multiphase Production* (Edited by BURNS, A. P.), pp. 19–21. Elsevier, London.

LANDMAN, M. J. 1991b Non-unique holdup and pressure drop in two-phase stratified inclined pipe flow. *Int. J. Multiphase Flow* **17,** 377–394.

LIN, P. Y. & HANRATTY, T. J. 1986 Prediction of the initiation of slugs with linear stability theory. *Int. J. Multiphase Flow* **12,** 79–98.

LIN, P. Y. & HANRATTY, T. J. 1987 Effect of pipe diameter on flow patterns for air–water flow in horizontal pipes. *Int. J. Multiphase Flow* **13,** 549–563.

MISHIMA, K. & ISHII, M. 1980 Theoretical prediction of onset of horizontal slug flow. *Trans. ASME Jl Fluids Engng* **102,** 441–445.

NICHOLSON, M. K., AZIZ, K. & GREGORY, G. A. 1978 Intermittent two phase flow in horizontal pipes: predictive models. *Can. J. Chem. Engng* **56,** 653–663.

RAMSHAW, J. D. & TRAPP, J. A. 1978 Characteristics, stability, and short-wavelength phenomena in two-phase equation system. *Nucl. Sci. Engng* **66,** 93–102.

SHOHAM, O. 1982 Flow pattern transitions and characterization in gas–liquid two phase flow in inclined pipes. Ph.D. Dissertation, Tel-Aviv Univ., Ramat-Aviv, Israel.

TAITEL, Y. & DUKLER, A. E. 1976 A model for prediction of flow regime transitions in horizontal and near horizontal gas–liquid flow. *AIChE Jl* **22,** 47–55.

TAITEL, Y. & DUKLER, A. E. 1987 Effect of pipe length on the transition boundaries for high viscosity liquids. *Int. J. Multiphase Flow* **13,** 577–581.

WALLIS, G. B. 1969 *One-dimensional Two-phase Flow*. McGraw-Hill, New York.

WALLIS, G. B. & DOBSON, J. E. 1973 The onset of slugging in horizontal stratified air–water flow. *Int. J. Multiphase Flow* **1,** 173.

WU, H. L., POTS, B. F. M., HOLLENBERG, J. F. & MEERHOFF, R. 1987 Flow pattern transitions in two-phase gas/condensate flow at high pressure in an 8-inch horizontal pipe. In *Proc. 3rd Int. Conf. on Multiphase Flow*, The Hague, The Netherlands, pp. 13–21.